Metabolomic analyses reveal profound differences in glycolytic and tricarboxylic acid cycle metabolism in glucose-responsive and -unresponsive clonal β-cell lines

Peter SPÉGEL[*], Siri MALMGREN[*,†], Vladimir V. SHAROYKO[*], Philip NEWSHOLME[‡], Thomas KOECK[*], and Hindrik MULDER[*]

Department of Clinical Sciences in Malmö, [*]Unit of Molecular Metabolism, [†]Unit of Diabetes and Endocrinology, Lund University Diabetes Centre, Malmö, Sweden. [‡]UCD School of Biomolecular and Biomedical Science, UCD Conway Institute and UCD Institute of Sport and Health, UCD Dublin, Belfield, Dublin 4, Ireland.

Running Head: Metabolic regulation in β-cells

Correspondence to: Peter Spégel, PhD, Malmö University Hospital, Clinical Research Center, 91:11:061, 205 02 Malmö, Sweden. Tel.: 0046 40 39-10-21; Fax: 0046 40 39-12-22; E-mail: Peter.Spegel@med.lu.se

Keywords: Hypoxia-induced factor, HIF, pancreatic islets, insulin, Type 2 Diabetes, mitochondria

Insulin secretion from pancreatic ß-cells is controlled by complex metabolic and energetic changes provoked by exposure to metabolic fuels. Perturbations in these processes lead to impaired insulin secretion, the ultimate cause of Type 2 Diabetes. To increase our understanding of stimulus-secretion coupling and metabolic processes potentially involved in the pathogenesis of Type 2 Diabetes, a comprehensive investigation of the metabolic response in the glucose-responsive INS-1 832/13 and glucose-unresponsive INS-1 832/2 β-cell lines was performed. For this metabolomics analysis, we used gas chromatography/mass spectrometry combined with multivariate statistics. We found that perturbed secretion in the 832/2 line was characterized by disturbed coupling of glycolytic and TCA-cycle metabolism. The importance of this metabolic coupling was reinforced by our observation that insulin secretion partially could be reinstated by stimulation of the cells with mitochondrial fuels which bypass glycolytic metabolism. Furthermore, metabolic and functional profiling of additional ß-cell lines (INS-1, INS-1 832/1) confirmed the important role of coupled glycolytic and TCA-cycle metabolism in stimulus-secretion coupling. Dependence of the unresponsive clones on glycolytic metabolism was paralleled by increased stabilization of hypoxia-induced factor 1α (HIF-1α). The relevance of a similar perturbation for human Type 2 Diabetes was suggested by increased expression of HIF-1α target genes in islets from Type 2 Diabetes patients.

INTRODUCTION

Failure of the pancreatic β-cells to release insulin appropriately is a major pathogenetic abnormality in Type 2 Diabetes. Insulin secretion from β-cells is controlled by two different mechanisms: the triggering (K_{ATP}-dependent) and the amplifying (K_{ATP}-independent) pathways [1]. While the triggering pathway has been thoroughly characterized [2, 3], the mechanisms and signals underlying the amplifying pathway remain largely unknown [4, 5]. Yet, several metabolites, mainly originating from mitochondrial metabolism, have been implicated as potential coupling factors in the amplifying pathway of glucose-stimulated insulin secretion (GSIS). These include long-chain acyl-CoAs [6], glutamate [7], and NADPH [8, 9].

In the present study, the metabolome of two clonal β-cell lines, the glucose-responsive 832/13 and the glucose-unresponsive 832/2 line, both derived from the INS-1 rat insulinoma cell line [10], were examined. This enabled us to investigate possible differences in metabolic regulation that underlie perturbed function of the 832/2 cells. Expression of several glycolytic and tricarboxylic acid (TCA) cycle enzymes has previously been found to differ between these cell lines [11]. Most strikingly, the 832/2 cells were found to express lactate dehydrogenase A (LDH-A) and release lactate. Hence, the glucose-unresponsive 832/2 line relied heavily on glycolytic metabolism, while the robust insulin secretor, the 832/13 line, exhibited strong glucose concentration-dependent coupling of cytosolic and mitochondrial fuel metabolism. Moreover, it has previously been shown that 832/13 cells are characterized by an active anaplerotic pathway, which is less pronounced in 832/2 cells [12]. Nevertheless, a detailed analysis of the impact of these metabolic differences on the levels of individual metabolites and how they are controlled has not yet been performed.

To date, the bulk of investigations on the coupling of β-cell metabolism to insulin secretion has been performed in a univariate fashion. One or a few metabolites or metabolic enzymes have been studied at a time. Due to the complexity of the metabolic networks, univariate investigations are likely to be insufficient. An unbiased characterization of metabolism is therefore warranted. Thus, in the present study, gas chromatography/mass spectrometry (GC/MS)-based metabolomics [13-15] combined with multivariate statistical analyses [16] were applied to investigate the metabolome. These metabolomic analyses generated hypotheses, which we aimed to verify with functional studies and analysis of human islets.

A prominent finding was the lacking response of levels of late glycolytic and TCA cycle intermediates in the unresponsive 832/2 cell line despite an increase in extracellular glucose. The perturbed coupling of cytosolic and mitochondrial metabolism could partially be circumvented by specifically stimulating mitochondrial metabolism. This manoeuvre reinstated fuel-stimulated mitochondrial respiration and insulin secretion. Interestingly, we found that hypoxia-inducible factor 1α (HIF-1α), a transcription factor regulating the balance between glycolytic and mitochondrial metabolism, was stabilized in the glucose-unresponsive cells.

EXPERIMENTAL

Metabolomics

Clonal ß-cell lines INS-1 832/2 and INS-1 832/13 were stimulated with either 2.8 or 16.7 mM glucose for 1 h followed by an unbiased analysis of the metabolome using GC/MS. The generated data were normalized and evaluated using multivariate statistics to highlight alterations in metabolite levels unique to or shared between the two cell lines. To validate the finding in the 832/2 and 832/13 clones, a metabolite profiling of the glucose responsive INS-1 and the glucose unresponsive INS-1 832/1 clones was undertaken. Details of the metabolomics protocols are found in the Supplemental information.

Insulin secretion

INS-1, 832/1, 832/2 and 832/13 clones were cultured in 24-well culture plates to reach 90-95 % confluency, whereafter insulin was assayed as previously described in detail [10]. Insulin secretion was measured after incubation for 1 h in 2.8 mM glucose, 16.7 mM glucose or 10 mM leucine and 10 mM glutamine.

Oxygen consumption
The oxygen consumption rate (OCR) was measured in the 832/2 and 832/13 clones using the Extracellular flux (XF) analyzer XF24 (Seahorse Bioscience, Billerica, MA), as previously described in detail [11]. Following a pre-incubation at 2.8 mM glucose for 2 h, the OCR was assayed at 2.8 mM glucose subsequent to a transition to 16.7 mM glucose or 2.8 mM glucose together with 10 mM leucine and 10 mM glutamine. OCRs were first normalized by protein content and then by the average basal OCR at 2.8 mM glucose. An area under the curve analysis was performed for fuel-stimulation conditions.

Glucose uptake
The cells were prepared as for analysis of insulin secretion [10]. After removing the secretion assay buffer (SAB), 500 µl of SAB containing 3-O-methyl-D-[3H(N)]glucose (specific activity, 80.2 Ci/mmol; PerkinElmer Life Sciences) and 3-O-methyl-D-glucose to a final concentration of 2.8 or 16.7 mM 3-O-methyl-D-glucose, respectively, were added to each well. Cells were incubated for 10 min at 37 °C. Next, 250 µl of lysis buffer containing 200 mM NaCl, 2 mM EDTA, 50 mM Tris-HCl (pH 7.4) and 1% SDS were added. Subsequently, 150 µl of lysate were transferred into scintillation vials. Protein content was determined by the bicinchoninic acid (BCA) method. 3-O-methyl-D-[3H(N)]glucose content was measured by liquid scintillation spectrometry [17].

Western blotting
Whole cells were solubilized in homogenization buffer (100 mM HEPES, 9 M urea, 1% Triton X-100, 2 mM EDTA, pH 7.2) mixed 1:100 (v/v) with protease inhibitor cocktail (Sigma, St. Louis, MO). Protein content was determined by the BCA method. Samples were mixed 1:10 (v/v) with loading buffer (100 mM HEPES, 10% SDS, 10% dithiothreitol, 20% glycerol, pH 7.2). 40 µg protein were run on an 8% SDS-PAGE gel, and subsequently blotted onto PVDF membranes. HIF-1α protein was detected with a primary mouse anti-HIF-1α monoclonal antibody (Abcam, Cambridge, UK) in dilution 1:500 (v/v). β-Tubulin was detected with a primary rabbit polyclonal antibody (Santa Cruz Biotechnology, Santa Cruz, CA, USA) in dilution of 1:400 (v/v). Horse-radish peroxidase-coupled goat-anti-rabbit IgG (1:8000, v/v), goat-anti-mouse IgG (1:6000, v/v), and donkey-anti-goat IgG (1:8000, v/v) (Santa Cruz Biotechnology, Santa Cruz, CA) were used as secondary antibodies. Blots were developed with enhanced chemiluminescence (ECL) and detection was by Amersham Hyperfilm ECL (Amersham Biosciences, Uppsala, SE). Films were scanned using the Bio-Rad GS-800 Calibrated Densitometer (Bio-Rad, Sundbyberg, SE). Measurements obtained for HIF-1α were corrected for protein loading with β-tubulin. For loading control blots were stripped with 2% SDS, 100 mM 2-mercaptoethanol, 62.5 mM Tris-HCl, pH 6.7.

Human islets
Human pancreatic islets from 55 non-diabetic and 9 T2D deceased donors were obtained from the Human Tissue Laboratory at Lund University Diabetes Centre. The 29 male and 26 female non-diabetic donors were aged 56.7± 9.8 years, had a BMI of 25.9 ± 3.6 kg/m^2 and HbA_1c of 5.7 ± 0.8. The 5 male and 4 female T2D donors were aged 57.0 ± 13.1 years, had a BMI of 28.5 ± 4.7 kg/m^2 and HbA_1c of 7.3 ± 1.2. Islets were prepared by collagenase digestion and density gradient purification. After isolation, islets were cultured free floating in CMRL 1066 culture medium (ICN Biomedicals, Costa Mesa, CA, USA) supplemented with 10 mmol/l HEPES, 2 mmol/l 1-glutamine, 50 µg/ml gentamicin, 0.25 µg/ml Fungizone (GIBCO BRL, Gaithersburg, MD, USA), 20 µg/ml ciprofloxacin (Bayer Healthcare, Leverkusen, Germany), and 10 mmol/l nicotinamide at 37°C (5% CO_2) prior to RNA and DNA preparation. The donor before death or her/his relatives upon admission to Intensive Care Unit (ICU) had given their consent to donate organs and the local ethics committees approved the protocols.

Total RNA was isolated with the AllPrep DNA/RNA Mini Kit (Qiagen GmbH, Hilden, Germany). The microarrays were performed following the Affymetrix standard protocol. Briefly, 200 ng total RNA were processed following the GeneChip® Expression 3'-Amplification Reagents One-cycle cDNA synthesis kit instructions (Affymetrix Inc, Santa Clara, CA, US) to produce double-stranded cDNA. This was used as a template to generate biotin-targeted cRNA following

manufacturer's specifications. 15 μg of the biotin labeled cRNA were fragmented to strands between 35 and 200 bases in length, 10 μg of which were hybridized onto the GeneChip® Human Gene 1.0 ST whole transcript based assay overnight in the GeneChip® Hybridization oven 6400 using standard procedures. The arrays were washed and stained in a GeneChip® Fluidics Station 450. Scanning was carried out with the GeneChip® Scanner 3000 and image analysis was performed using GeneChip® Operating Software. The array data were summarized and normalized with Robust Multi-array Analysis (RMA) method using the software "Expression Console" (Affymetrix).

Statistical analysis

All data are shown as mean ± standard deviation or standard error of the mean for indicated number of experiments. A Mann-Whitney U-test was used to compare data from human islets. Unless stated otherwise, Student's t-test was used when comparing two groups. The Kruskal-Wallis test in combination with Mann-Whitney followed by Bonferroni´s test *post hoc* was applied for the analysis of HIF-1α protein expression.

RESULTS

Metabolomics

Multivariate statistical calculations were performed to identify which metabolites out of the 164 detected were uniquely regulated by the glucose stimulation in the INS-1 832/2 and the INS-1 832/13 clones (see Supplemental information). These analyses revealed a unique regulation of the late glycolytic and TCA-cycle intermediates in the 832/13 clone (Figure 1A and B). Whereas glucose-6-phosphate was found to exhibit a glucose-stimulated increase in both cell lines, downstream intermediates 3-phosphoglycerate, 2-phosphoglycerate, phosphoenolpyruvate and pyruvate were found to increase exclusively in the glucose responsive 832/13 clone. This lack of response in the 832/2 clone was reflected also by the levels of the TCA-cycle intermediates; levels of all measured TCA-cycle intermediates increased in the 832/13 clone whereas they were unaltered in the 832/2 clone (Figure 1B). The fold of the glucose-stimulated increase in lactate was similar in the two clones (Figure 1A), although the levels were significantly higher in the un-responsive clone (see Supplementary Figures S4 and S8). The level of the pentose phosphate shunt intermediate ribose-5-phosphate rose more in the glucose responsive 832/13 clone.

Oxygen consumption

Given the lack of rise in TCA-cycle intermediates in the 832/2 clone in response to glucose, we were interested to find out whether this had any further functional implications. To this end, we chose to assess oxygen consumption, which reflects overall mitochondrial activity. Based on an area under the curve analysis, glucose stimulation caused a sustained 1.84 ± 0.26-fold (n=7) increase in OCR in the 832/13-clone, whereas no change in OCR was observed upon glucose stimulation of the 832/2-clone (Figure 2A,C). However, leucine and glutamine increased the OCR in both clones; OCR was significantly increased 1.81 ± 0.18-fold (n=6) and 1.26 ± 0.07-fold (n=6) in 832/13 and 832/2 cells, respectively (Figure 2B,C), compared with respiration at 2.8 mM glucose alone.

Insulin secretion

The lack of a glucose-stimulated response in levels of TCA-cycle intermediates in the glucose-unresponsive 832/2 clone is likely to constrain insulin secretion via both the triggering pathway, which is dependent on the mitochondrial ATP production, and the amplifying pathway, which has been suggested to be coupled to TCA-cycle metabolism. Basal insulin secretion at 2.8 mM glucose was 15.9 ± 1.8 (n=8) and 8.39 ± 1.96 (n=6) ng/mg/h for 832/13 and 832/2 cells, respectively. Indeed, while stimulation with 16.7 mM glucose yielded a 12.6 ± 1.3-fold (n=8) increase of insulin secretion in the glucose-responsive 832/13 cell, no rise in GSIS was observed in the glucose-unresponsive 832/2 line (Figure 2D). Leucine and glutamine, on the other hand, significantly stimulated insulin secretion in 832/2 cells (2.88 ± 0.22-fold (n=6) increase vs. basal), whereas the same stimulus yielded a 14.1 ± 5.5-fold (n=6) increase in the glucose-responsive 832/13 line (Figure 2D).

Metabolite profiling of additional clonal ß-cell lines

The results generated from the study of the glucose responsive 832/13-clone and the glucose unresponsive 832/2 clone suggested that insufficient coupling of glycolytic and TCA-cycle metabolism may be a factor underlying perturbed GSIS. To investigate whether this phenotype is unique for the glucose unresponsiveness of the 832/2 clone or a more general phenomenon in ß-cells, two additional ß-cell lines were investigated. To this end, the glucose-responsive INS-1 line and the glucose-unresponsive INS-1 832/1 sub-clone were examined. A targeted metabolite profiling revealed a significantly lower fold-change of glucose-stimulated alterations in glycolytic and TCA-cycle metabolite levels in the unresponsive clone (Figure 3), reminiscent of the metabolic phenotype of the 832/2 clone (Figure 1A-B).

Functional characterization of additional clonal ß-cell lines

Next, the functional consequences of the reduced response in the glycolytic and TCA-cycle intermediates upon glucose stimulation were assessed. Glucose was found to stimulate insulin secretion 6.6±2.6 fold (n=3) in the INS-1 parental clone, whereas insulin secretion from the 832/1 sub-clone was not stimulated by the hexose (1.2±0.3 fold, n=3). To investigate whether stimulus secretion coupling was intact and the observed lack of response in the 832/1 clone was due to insufficient coupling of glycolytic and TCA-cycle metabolism, insulin secretion in response to leucine and glutamine was also assessed. Indeed, leucine and glutamine provoked a significant ($p<0.05$) 7.8±2.4 fold and a 3.1±1.0 fold increase in insulin secretion in the INS-1 and the 832/1-clone, respectively.

Glucose uptake

To investigate whether differences in glucose uptake could account for the observed metabolic differences between the glucose-responsive and -unresponsive ß-cell clones, uptake of the non-metabolizable analogue of D-glucose, 3-O-methyl-D-glucose, was assessed. No significant differences between the four clones could be observed (see Supplementary Figure S9), indicating that differences in glucose uptake alone can not explain the perturbed metabolic response in the glucose unresponsive clones.

Stabilization of HIF-1α

The metabolomics data suggested that the lacking response of the 832/2-clone to glucose stimulation may be caused by impaired aerobic glycolysis concurrent with lactate production and a perturbation in the coupling between cytosolic and TCA-cycle metabolism. This together with the fact that the cell-lines are tumour derived [10] suggested involvement of HIF-1α. Stabilization of this protein may account for a switch of cellular metabolism to dependence on glycolysis, the so called Warburg-effect [18]. To explore this possibility, we determined the presence of HIF-1α by Western blotting. Indeed, while HIF-1α was present in all INS-1 clones, its protein levels were e.g. 227 ± 30 % ($p=0.006$) higher in the glucose-unresponsive 832/2 clone, in comparison to the glucose-responsive 832/13 clone (Figure 4A-B).

It has recently been shown that a low level of α-ketoglutarate in the presence of a high level of succinate stabilizes HIF-1α [19, 20]. To assess whether such a mechanism is operating in the clonal cell lines, we plotted the HIF-1α protein levels against the ratios of α-ketoglutarate and succinate (fold responses of the metabolite levels to glucose stimulation were employed; Figure 4C). Indeed, we observed that the lower the ratios of α-ketoglutarate to succinate, the higher the protein level of HIF-1α. Next, we examined whether the change in HIF-1α protein levels coincided with metabolic changes. To this end, we plotted HIF-1α protein levels against the ratios of citrate to pyruvate (Figure 4D). The rationale for this analysis is that this ratio may reflect coupling of glycolysis and TCA-cycle activities. A low ratio would imply a low level of TCA-cycle activity, suggesting that coupling of glycolysis and TCA-cycle is perturbed. The plot clearly shows that high HIF-1α protein levels coincided with a low ratio of citrate to pyruvate in the clonal ß-cell-lines. This translated into impaired GSIS, as shown in figure 4E.

Expression of HIF-1α target genes in human islets

Stabilization of HIF-1α can establish a pseudo-hypoxic metabolic phenotype under normoxic conditions. This involves primarily increased expression of glycolytic enzymes. Thus, to investigate whether our findings in the clonal cell-lines are of relevance for the pathogenesis of Type 2 Diabetes in humans, we first analyzed expression of HIF-1α in human islets. Although HIF-1α was expressed at the mRNA-level, we did not observe any differences between human islets from healthy controls and patients with Type 2 Diabetes (data not shown). This is in agreement with the fact that signalling through HIF-1α requires stabilisation on the protein level, a phenomenon which occurs independent of changes in mRNA-level of HIF-1α [21]. Instead, to ascertain whether regulation by HIF-1α occurs in human islets, we examined expression of HIF-1α target genes in human islets from healthy controls and patients with Type 2 Diabetes. Indeed, we found increased mRNA levels for hexokinase 2, lactate dehydrogenase, and phosphofructokinase-2/fructose-2,6-bisphosphatase-3. Unexpectedly, there were minor, but significant, decreases in pyruvate dehydrogenase kinase-1 (~13%) and enolase (~22%) mRNA levels.

DISCUSSION

The complexity of β-cell metabolism prompts novel analytical approaches that allow analyses of more than one or a few metabolites at time. In the present study, metabolomics allowed the simultaneous analysis of 164 putative metabolites, out of which 44 could be identified. Analyses of four clonal β-cell-lines with variable glucose responsiveness and hence stimulated insulin secretion pinpointed a fundamental disruption of metabolism in the glucose-unresponsive clones. The disruption appeared to be at the level of coupling glycolysis to TCA-cycle metabolism. As metabolism moved down the path of glycolysis, the weaker the glucose-stimulated response in metabolite levels became. In fact, even lactate, a metabolite not thought to be compatible with robust β-cell function, was increasingly produced in glucose-unresponsive cell-lines [11].

To explore whether this observed metabolic perturbation impacted mitochondrial activity, we analyzed OCR in presence of either glucose, which requires glycolytic metabolism, or a combination of leucine and glutamine, which directly activates TCA-cycle metabolism. In agreement with the metabolomics data, glucose was ineffective to stimulate oxygen consumption in glucose-unresponsive cells with the observed block of coupling between glycolysis and TCA-cycle metabolism. In contrast, fuels that were directly metabolized in the TCA-cycle increased oxygen consumption also in glucose-unresponsive cells, albeit not to the same extent as in glucose-responsive cells. This suggests that TCA-cycle metabolism and oxidative phosphorylation in the glucose-unresponsive cell-lines have adapted to a metabolic situation where provision of fuels from glycolysis is constrained. In support of this notion, we have previously shown that respiratory complex activities and protein expression of key subunits of the complexes are decreased in 832/2 versus 832/13 cells [11]. Nevertheless, when mitochondrial fuels are provided, a metabolic response from mitochondria can still be provoked. Accordingly, fuels metabolized directly in the TCA-cycle were able to stimulate insulin secretion also in the clones totally lacking a secretory response to glucose.

At this point, the question remained how the adaptive transition from coupled glycolytic and TCA-cycle metabolism to an increasing dependence on glycolysis was regulated. As we previously observed [11], metabolism in the 832/2 line exhibits Warburg-like features. Moreover, the metabolite profiling revealed that TCA-cycle intermediates, particularly succinate, that can inhibit proline hydroxylases when coinciding with low levels of α-ketoglutarate, were increasingly abundant in cells with low glucose responsiveness. Proline hydroxylases hydroxylate HIF-1α, priming it for proteolytic degradation. The inhibition of this process is an important component of the Warburg transition establishing a pseudohypoxic normoxic condition. HIF-1α serves a transcription factor, enhancing expression of genes in the glycolytic pathway. Hereby energy homeostasis is maintained under hypoxic conditions, a situation commonly found in tumour-derived cells even under normoxic conditions. Indeed, the cell lines examined in this study are of tumour origin, originally derived from a transplantable rat insulinoma [22]. Accordingly, we found that HIF-1α protein was present in all the clonal cell lines, being most abundant in the cell lines with the lowest level of glucose responsiveness. In support of this observation, we found that increased levels of HIF-1α protein coincided with a perturbed coupling of glycolysis and TCA-cycle metabolism as evident from the citrate to pyruvate

ratio. Moreover, higher HIF-1α protein levels corresponded to impaired GSIS. Collectively, these observations suggest that HIF-1α is a key regulator of the balance between glycolytic and TCA-cycle metabolism in β-cells. In this capacity, HIF-1α could serve as a regulator of β-cell stimulus-secretion coupling. However, while our experiments have established a relation between HIF-1α and glucose responsiveness, it remains to be shown that this is a casual effect. Supporting a casual relationship are recent findings showing that genetic targeting of the von Hippel-Lindau factor in mouse β-cells stabilizes HIF-1α resulting in impaired glucose tolerance and perturbed insulin secretion [23]. Yet another study shows that HIF-1α present at low levels in mouse β-cells under normoxic conditions is required for proper β-cell function [24]. This circumstance could explain why we also found HIF-1α protein in the glucose-responsive cell-lines, albeit at very low levels.

The relevance of our findings for the pathogenesis of Type 2 Diabetes is supported by studies of animal models for the disease. For instance, lactate production has been shown to be increased in the Goto-Kakizaki (GK) rat [25]. Moreover, it has previously been shown that leucine-stimulated glutamate metabolism is intact in the GK rat and that the combination of these amino acids stimulates insulin secretion [26]; the latter is reminiscent of what we observed in the glucose-unresponsive cell lines. In fact, although patients with Type 2 Diabetes exhibit severely perturbed GSIS, glutamine-leucine-stimulated insulin secretion is largely preserved [27]. Substantiating our findings on HIF-1α, it has previously been reported that the protein is expressed in human islets [24]. Using our repository of human islets, we could confirm this finding. However, there was no difference between patients with Type 2 Diabetes and healthy controls. This was no surprise given that HIF-1α mRNA levels are not thought to contribute to its regulatory function. Instead, this is controlled by its stabilization at the protein level. Therefore, we explored expression of HIF-1α target genes in human islets. Indeed, we found that some of the known targets of this transcription factor, e.g. hexokinase 2, lactate dehydrogenase, and 6-phosphofructo-2-kinase/fructose-2,6-bisphosphatase-3 were up-regulated in islets from patients with Type 2 Diabetes. While these data are compelling, there should be call for caution. The human islets used in our studies, as well as in any other studies, have been cultured for different lengths of time. In this situation, the circulation in the islets has been compromised. This implies that hypoxia may prevail in these islets, particularly in the core of the islets. Clearly, such hypoxia could stabilize HIF-1α. This notwithstanding, we did observe a difference between healthy controls and patients with Type 2 Diabetes.

In conclusion, we have used metabolomics analysis to identify a profound perturbation in stimulus-secretion coupling in clonal β-cells. The metabolite profile suggested to us that HIF-1α could play a role in the observed transition of metabolism to dependence on glycolysis. The functional studies as well as observations in human islets suggest that an improper alignment of glycolysis with TCA-cycle metabolism may underlie perturbed GSIS. As such it may play a role in the pathogenesis of human Type 2 Diabetes. Further work is required to establish a casual relationship of these phenomena.

AUTHOR CONTRIBUTION

Peter Spégel performed metabolomics analyses and wrote the first draft of the manuscript. Siri Malmgren performed insulin secretion and oxygen consumption measurements. Vladimir Sharoyko performed glucose uptake measurement, provided feedback on results and the manuscript and, assisted in metabolite extraction. Thomas Koeck determined HIF-1α stabilization, performed oxygen consumption measurements, and provided feedback on results and the manuscript. Philip Newsholme provided feedback on results and the manuscript throughout the project. Hindrik Mulder conceived and directed the project and finalized the paper.

ACKNOWLEDGEMENTS

We thank the Nordic Center for Islet Transplantation in Uppsala, Sweden for providing us with human islets. Charlotte Ling is acknowledged for analyzing expression data from human islets, and Jalaal Taneera and Thomas Lang for performing the microarray analyses.

FUNDING
This work was supported by grants from Swedish Research Council (14196-06-3), the Crafoord Foundation, the European Foundation for the Study of Diabetes, Lars Hierta, Fredrik and Ingrid Thuring, Åke Wiberg, Albert Påhlsson, O.E. and Edla Johansson Foundations, Knut and Alice Wallenberg Foundation, the Royal Physiographic Society, Lund University Diabetes Centre, and the Faculty of Medicine at Lund University. Support from Inga and John Hain Foundation to PS is acknowledged.

REFERENCES
1 Henquin, J. C. (2000) Triggering and amplifying pathways of regulation of insulin secretion by glucose. Diabetes. **49**, 1751-1760
2 Ashcroft, F. M., Proks, P., Smith, P. A., Ammala, C., Bokvist, K. and Rorsman, P. (1994) Stimulus-secretion coupling in pancreatic beta cells. Journal of cellular biochemistry. **55 Suppl**, 54-65
3 Berggren, P. O. and Larsson, O. (1994) Ca2+ and pancreatic B-cell function. Biochemical Society transactions. **22**, 12-18
4 Gembal, M., Gilon, P. and Henquin, J. C. (1992) Evidence that glucose can control insulin release independently from its action on ATP-sensitive K+ channels in mouse B cells. The Journal of clinical investigation. **89**, 1288-1295
5 Aizawa, T., Sato, Y., Ishihara, F., Taguchi, N., Komatsu, M., Suzuki, N., Hashizume, K. and Yamada, T. (1994) ATP-sensitive K+ channel-independent glucose action in rat pancreatic beta-cell. The American journal of physiology. **266**, C622-627
6 Prentki, M., Vischer, S., Glennon, M. C., Regazzi, R., Deeney, J. T. and Corkey, B. E. (1992) Malonyl-CoA and long chain acyl-CoA esters as metabolic coupling factors in nutrient-induced insulin secretion. The Journal of biological chemistry. **267**, 5802-5810
7 Maechler, P. and Wollheim, C. B. (1999) Mitochondrial glutamate acts as a messenger in glucose-induced insulin exocytosis. Nature. **402**, 685-689
8 Ivarsson, R., Quintens, R., Dejonghe, S., Tsukamoto, K., in 't Veld, P., Renstrom, E. and Schuit, F. C. (2005) Redox control of exocytosis: regulatory role of NADPH, thioredoxin, and glutaredoxin. Diabetes. **54**, 2132-2142
9 Ronnebaum, S. M., Ilkayeva, O., Burgess, S. C., Joseph, J. W., Lu, D., Stevens, R. D., Becker, T. C., Sherry, A. D., Newgard, C. B. and Jensen, M. V. (2006) A pyruvate cycling pathway involving cytosolic NADP-dependent isocitrate dehydrogenase regulates glucose-stimulated insulin secretion. The Journal of biological chemistry. **281**, 30593-30602
10 Hohmeier, H. E., Mulder, H., Chen, G., Henkel-Rieger, R., Prentki, M. and Newgard, C. B. (2000) Isolation of INS-1-derived cell lines with robust ATP-sensitive K+ channel-dependent and -independent glucose-stimulated insulin secretion. Diabetes. **49**, 424-430
11 Malmgren, S., Nicholls, D. G., Taneera, J., Bacos, K., Koeck, T., Tamaddon, A., Wibom, R., Groop, L., Ling, C., Mulder, H. and Sharoyko, V. V. (2009) Tight coupling between glucose and mitochondrial metabolism in clonal beta-cells is required for robust insulin secretion. The Journal of biological chemistry. **284**, 32395-32404
12 Lu, D., Mulder, H., Zhao, P., Burgess, S. C., Jensen, M. V., Kamzolova, S., Newgard, C. B. and Sherry, A. D. (2002) 13C NMR isotopomer analysis reveals a connection between pyruvate cycling and glucose-stimulated insulin secretion (GSIS). Proceedings of the National Academy of Sciences of the United States of America. **99**, 2708-2713
13 Fiehn, O. (2002) Metabolomics--the link between genotypes and phenotypes. Plant molecular biology. **48**, 155-171
14 Kopka, J. (2006) Current challenges and developments in GC-MS based metabolite profiling technology. Journal of biotechnology. **124**, 312-322
15 Fernandez, C., Fransson, U., Hallgard, E., Spegel, P., Holm, C., Krogh, M., Warell, K., James, P. and Mulder, H. (2008) Metabolomic and proteomic analysis of a clonal insulin-producing beta-cell line (INS-1 832/13). Journal of proteome research. **7**, 400-411
16 Trygg, J., Holmes, E. and Lundstedt, T. (2007) Chemometrics in metabonomics. Journal of proteome research. **6**, 469-479
17 Malaisse, W. J., Giroix, M. H., Malaisse-Lagae, F. and Sener, A. (1986) 3-O-methyl-D-glucose transport in tumoral insulin-producing cells. Am J Physiol. **251**, C841-846

18 Warburg, O. (1956) On the origin of cancer cells. Science. **123**, 309-314
19 Mole, D. R., Schlemminger, I., McNeill, L. A., Hewitson, K. S., Pugh, C. W., Ratcliffe, P. J. and Schofield, C. J. (2003) 2-oxoglutarate analogue inhibitors of HIF prolyl hydroxylase. Bioorg Med Chem Lett. **13**, 2677-2680
20 MacKenzie, E. D., Selak, M. A., Tennant, D. A., Payne, L. J., Crosby, S., Frederiksen, C. M., Watson, D. G. and Gottlieb, E. (2007) Cell-permeating alpha-ketoglutarate derivatives alleviate pseudohypoxia in succinate dehydrogenase-deficient cells. Mol Cell Biol. **27**, 3282-3289
21 Lendahl, U., Lee, K. L., Yang, H. and Poellinger, L. (2009) Generating specificity and diversity in the transcriptional response to hypoxia. Nat Rev Genet. **10**, 821-832
22 Asfari, M., Janjic, D., Meda, P., Li, G., Halban, P. A. and Wollheim, C. B. (1992) Establishment of 2-mercaptoethanol-dependent differentiated insulin-secreting cell lines. Endocrinology. **130**, 167-178
23 Cantley, J., Grey, S. T., Maxwell, P. H. and Withers, D. J. (2010) The hypoxia response pathway and beta-cell function. Diabetes Obes Metab. **12 Suppl 2**, 159-167
24 Cheng, K., Ho, K., Stokes, R., Scott, C., Lau, S. M., Hawthorne, W. J., O'Connell, P. J., Loudovaris, T., Kay, T. W., Kulkarni, R. N., Okada, T., Wang, X. L., Yim, S. H., Shah, Y., Grey, S. T., Biankin, A. V., Kench, J. G., Laybutt, D. R., Gonzalez, F. J., Kahn, C. R. and Gunton, J. E. (2010) Hypoxia-inducible factor-1alpha regulates beta cell function in mouse and human islets. J Clin Invest. **120**, 2171-2183
25 Ling, Z.-C., Efendic, S., Wibom, R., Abdel-Halim, S. M., Östenson, C.-G., Landau, B. R. and Khan, A. (1998) Glucose metabolism in Goto-Kakizaki rat islets. Endocrinology. **139**, 2670-2675
26 Giroix, M.-H., Saulnier, C. and Portha, B. (1999) Decreased pancreatic islet response to L-leucine in the spontaneously diabetic GK rat: enzymatic, metabolic and secretory data. Diabetologia. **42**, 965-977
27 Fernandez-Alvarez, J., Conget, I., Rasschaert, J., Sener, A., Gomis, R. and Malaisse, W. J. (1994) Enzymatic, metabolic and secretory patterns in human islets of Type 2 (non-insulin-dependent) diabetic patients. Diabetologia. **37**, 177-181
28 Eto, K., Tsubamoto, Y., Terauchi, Y., Sugiyama, T., Kishimoto, T., Takahashi, N., Yamauchi, N., Kubota, N., Murayama, S., Aizawa, T., Akanuma, Y., Aizawa, S., Kasai, H., Yazaki, Y. and Kadowaki, T. (1999) Role of NADH shuttle system in glucose-induced activation of mitochondrial metabolism and insulin secretion. Science (New York, N.Y. **283**, 981-985

FIGURE LEGENDS

Figure 1 Glucose-stimulated fold changes in metabolite levels.
Fold changes of metabolite levels after glucose stimulation were calculated by dividing the peak areas for the metabolite levels at 16.7 and 2.8 mM glucose derived from the glucose-unresponsive INS-1 832/2 and the glucose-responsive INS-1 832/13 lines, respectively. (**A**) Glycolytic and related metabolites. (**B**) TCA-cycle and related intermediates. The data are represented as mean±SEM. Statistical comparisons were made by t-test (*p<0.05, **p<0.01, ***p<0.001). Abbreviations: Rib5P - ribose-5-phosphate; Glu6P1 - glucose-6-phosphate peak 1; Glu6P2 - glucose-6-phosphate peak 2; GlyA3P - 3-phosphoglycerate; GlyA2P - 2-phosphoglycerate; PEP - phosphoenol pyruvate; Pyr - pyruvate; Lac - lactate; Cit - citrate; Aco - aconitate; AKGA - α-ketoglutarate; Succ - succinate; Fum - fumarate; Mal - malate.

Figure 2 Respiration and insulin secretion in glucose-responsive 832/13 and glucose-unresponsive 832/2 cells.
Oxygen consumption rate (OCR) in INS-1 832/13 (closed triangles) and 832/2 (open triangles) cells after addition of metabolic fuels. (**A**) 16.7 mM glucose or (B) 10 mM leucine + 10 mM glutamine. (**C**) Fuel-stimulated OCR during the stimulation period normalized to protein content and basal OCR at 2.8 mM glucose; calculated based on an area under curve (AUC) analysis [28]. (**D**) Fold-change of insulin secretion in INS-1 832/13 and INS-1 832/2 β-cells at 16.7 mM glucose and 10 mM of leucine + 10 mM of glutamine relative 2.8 mM glucose. Data are presented as means ±SEM (*p<0.05, **p<0.01, ***p<0.001).

Figure 3 Targeted metabolite profiling of the glucose –responsive INS-1 parental clone and the glucose-unresponsive INS-1 832/1 sub-clone.
A targeted metabolite profiling was performed to investigate whether the observed metabolic perturbation was present also in other clonal ß-cell lines. Fold-changes were calculated and compared as described in legend to Figure 1; (*p<0.05, **p<0.01, ***p<0.001). Abbreviations as in Figure 1.

Figure 4 Stabilization and functional relations of HIF-1α with metabolic and functional parameters in clonal ß-cell lines.
HIF-1α stabilisation was examined by Western-blotting as described in Experimental Procedures. n=3-6; data were compared by Kruskal-Wallis test in combination with Mann-Whitheny test followed by Bonferroni's test *post hoc*. **(A)** Western blot data. **(B)** Quantified levels of HIF-1α**. (C)** Stabilization of HIF-1α in relation to the ratio of α-ketoglutarate (AKGA) to succinate (Succ) (calculated as the ratio of their fold-changes to stimulatory glucose). **(D)** Stabilization of HIF-1α in relation to fold-changes of citrate (Cit) to pyruvate (Pyr) (see **C**). **(E)** Relationship between the fold-change of GSIS and HIF-1α stabilization.

Figure 5 Islet mRNA expression from patients with Type 2 Diabetes and healthy controls.
Expression of islet mRNA, derived from microarray analysis, of hexokinase 2 (HK2), enolase (ENO2), phosphofructokinase-2/fructose-2,6-bisphosphatase-3 (PFKFB3), pyruvate dehydrogenase kinase-1 (PDK1), and lactate dehydrogenase (LDHA). Data are given as means ± standard deviation and were compared with a Mann-Whitney U-test; (*p<0.05, **p<0.01, ***p<0.001).

Figure 6 Cartoon of the suggested involvement of HIF-1α in ß-cell stimulus-secretion coupling.
The cartoons show the proposed different modes of metabolic regulation in the glucose-responsive and -unresponsive clonal ß-cell lines involving hypoxia-induced factor 1α (HIF-1α). α-ketoglutarate – AKGA; hypoxia response element – HRE; lactate dehydrogenase – LDH; mitochondrion – M; nucleus – N; proline hydroxylases – PHD; pyruvate dehydrogenase – PDH; PDH kinase 1 – PDK1; oxidative phosphorylation – OXPHOS; succinate – suc; tricarboxylic acid cycle – TCA; von Hippel-Lindau factor – VHL

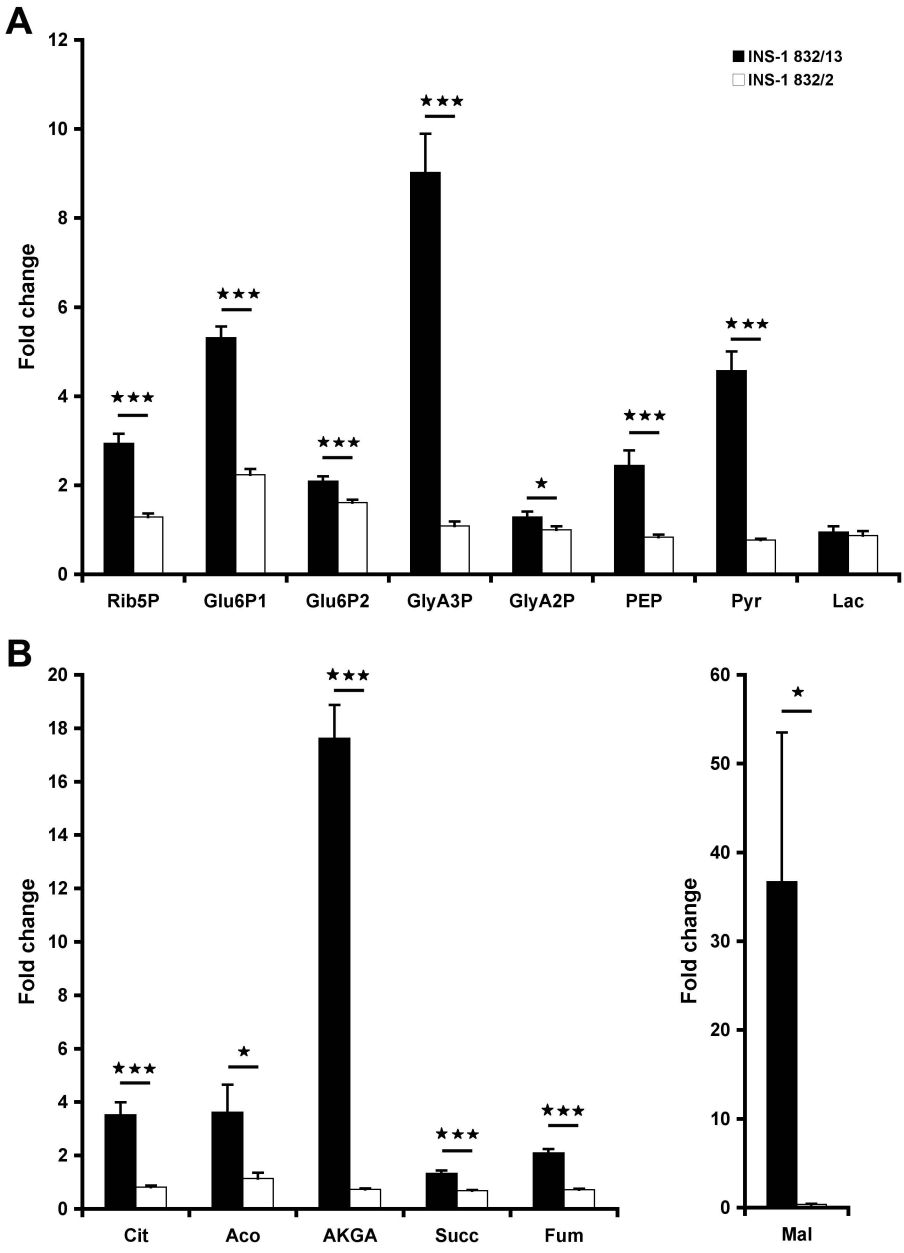
A
INS-1 832/13
INS-1 832/2
Fold change
0
2
4
6
8
10
12
Rib5P
Glu6P1
Glu6P2
GlyA3P
GlyA2P
PEP
Pyr
Lac
B
Fold change
0
2
4
6
8
10
12
14
16
18
20
Cit
Aco
AKGA
Succ
Fum
Fold change
0
10
20
30
40
50
60
Mal

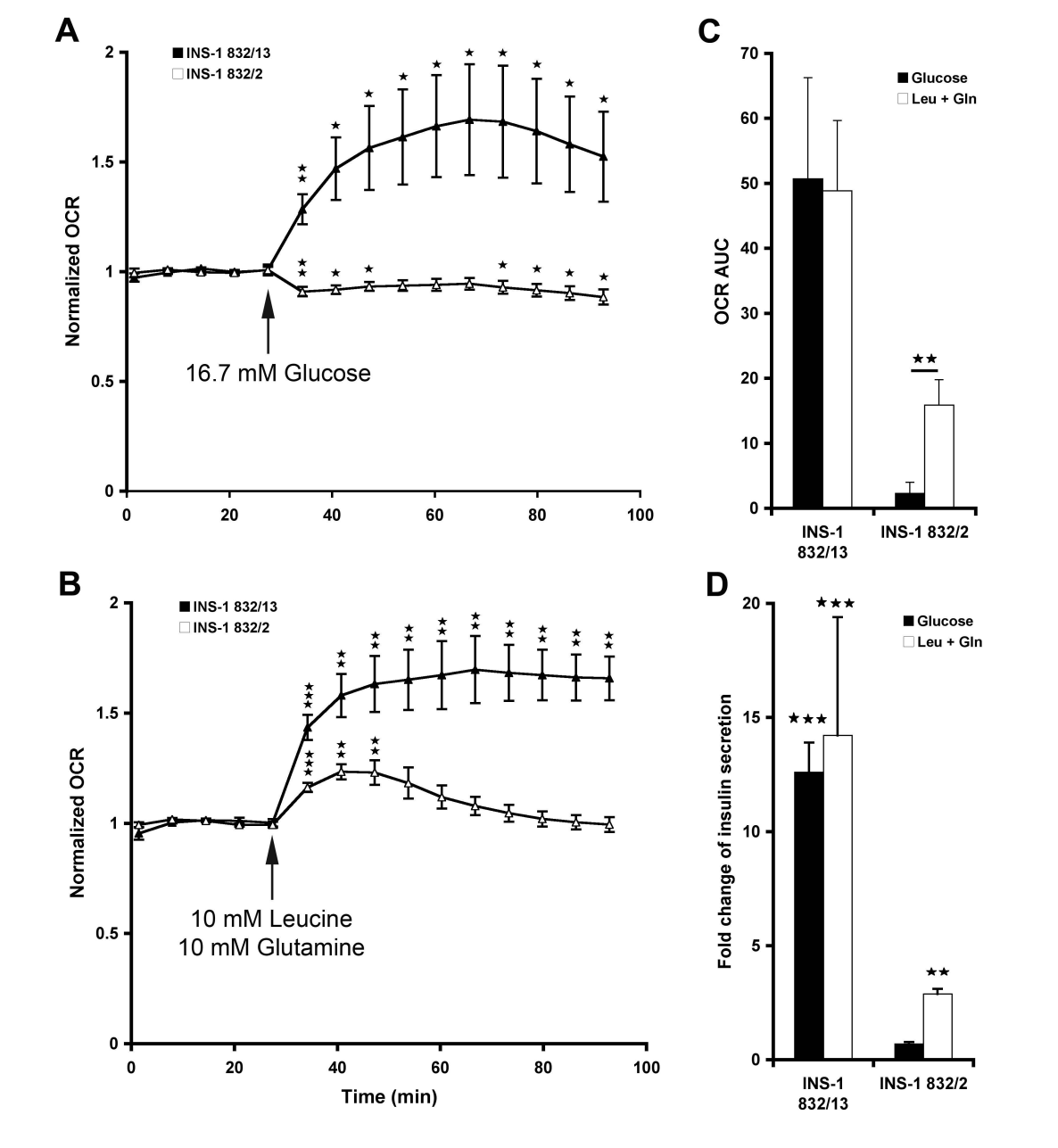
A
INS-1 832/13
INS-1 832/2
Normalized OCR
16.7 mM Glucose
B
INS-1 832/13
INS-1 832/2
Normalized OCR
10 mM Leucine
10 mM Glutamine
Time (min)
C
Glucose
Leu + Gln
OCR AUC
INS-1 832/13
INS-1 832/2
D
Glucose
Leu + Gln
Fold change of insulin secretion
INS-1 832/13
INS-1 832/2

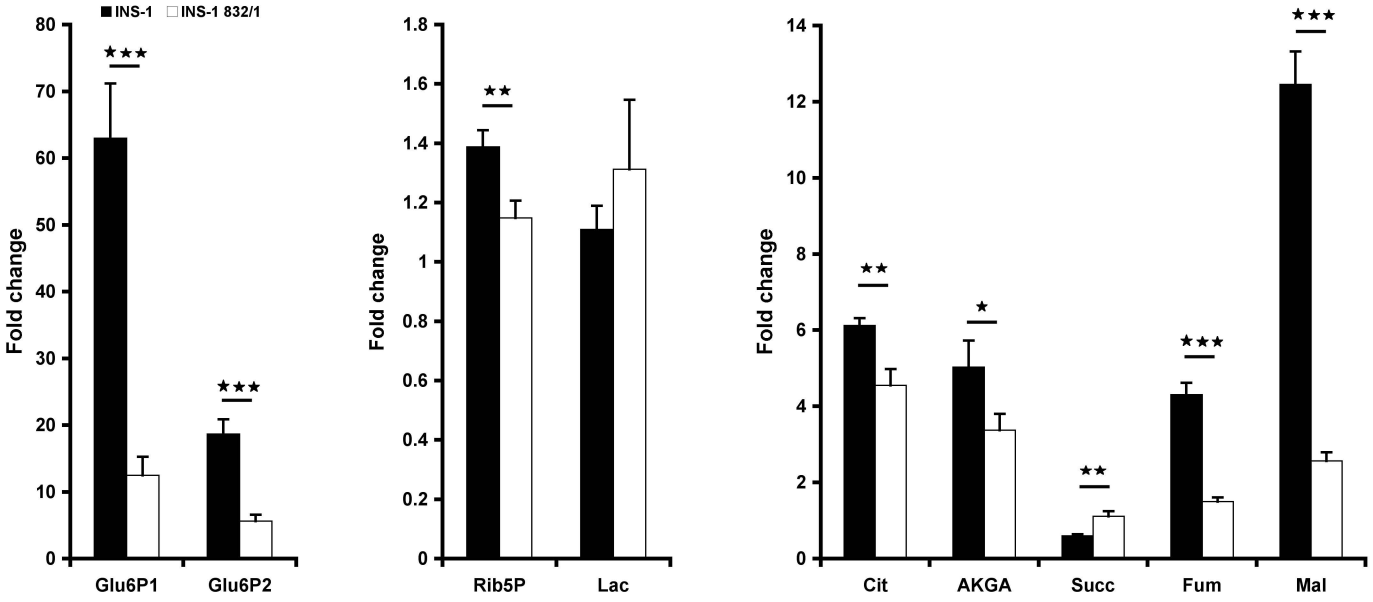
INS-1
INS-1 832/1
Fold change
Glu6P1
Glu6P2
Rib5P
Lac
Cit
AKGA
Succ
Fum
Mal

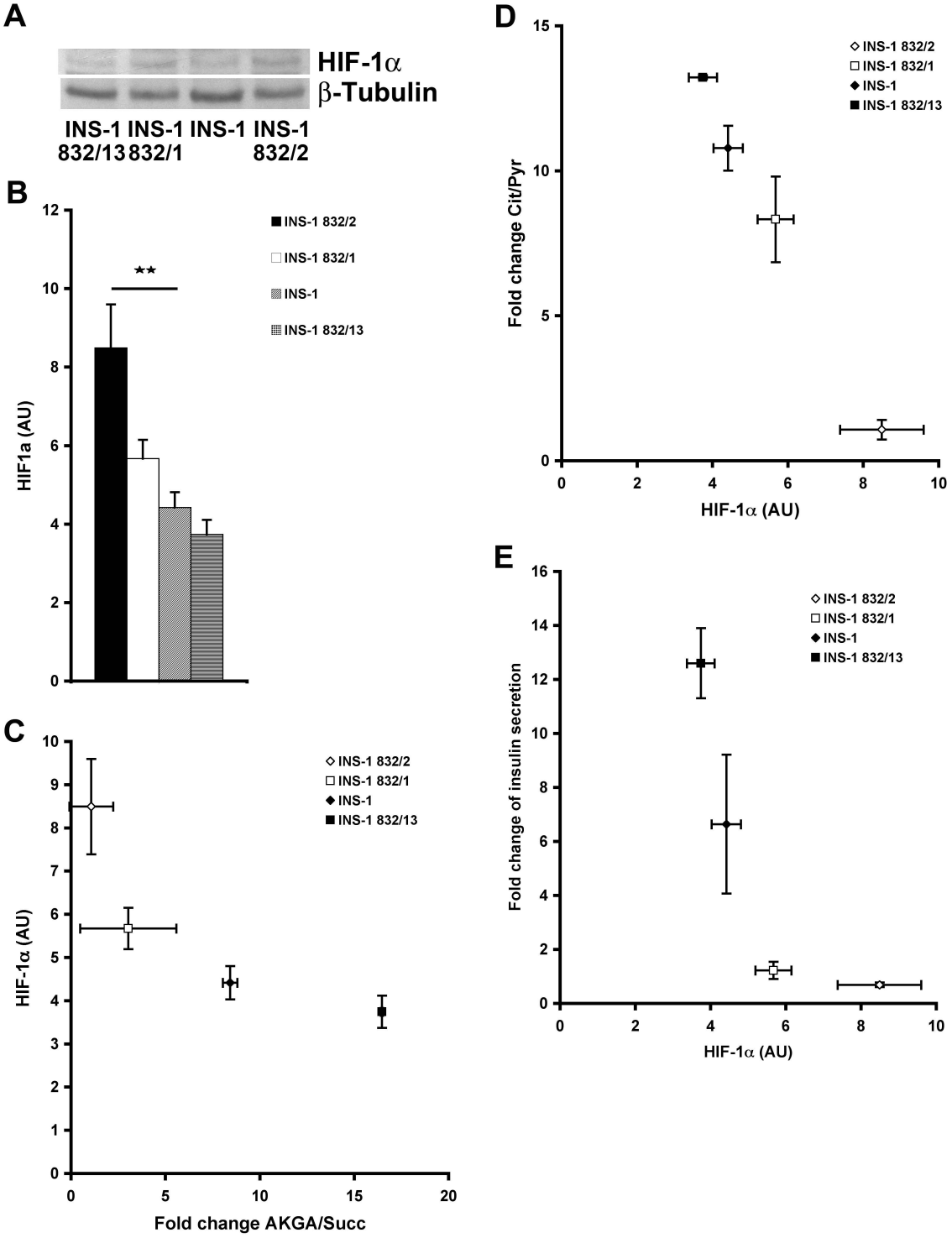
A
HIF-1α
β-Tubulin
INS-1 832/13
INS-1 832/1
INS-1
INS-1 832/2
B
HIF1a (AU)
**
INS-1 832/2
INS-1 832/1
INS-1
INS-1 832/13
C
HIF-1α (AU)
Fold change AKGA/Succ
INS-1 832/2
INS-1 832/1
INS-1
INS-1 832/13
D
Fold change Cit/Pyr
HIF-1α (AU)
INS-1 832/2
INS-1 832/1
INS-1
INS-1 832/13
E
Fold change of insulin secretion
HIF-1α (AU)
INS-1 832/2
INS-1 832/1
INS-1
INS-1 832/13

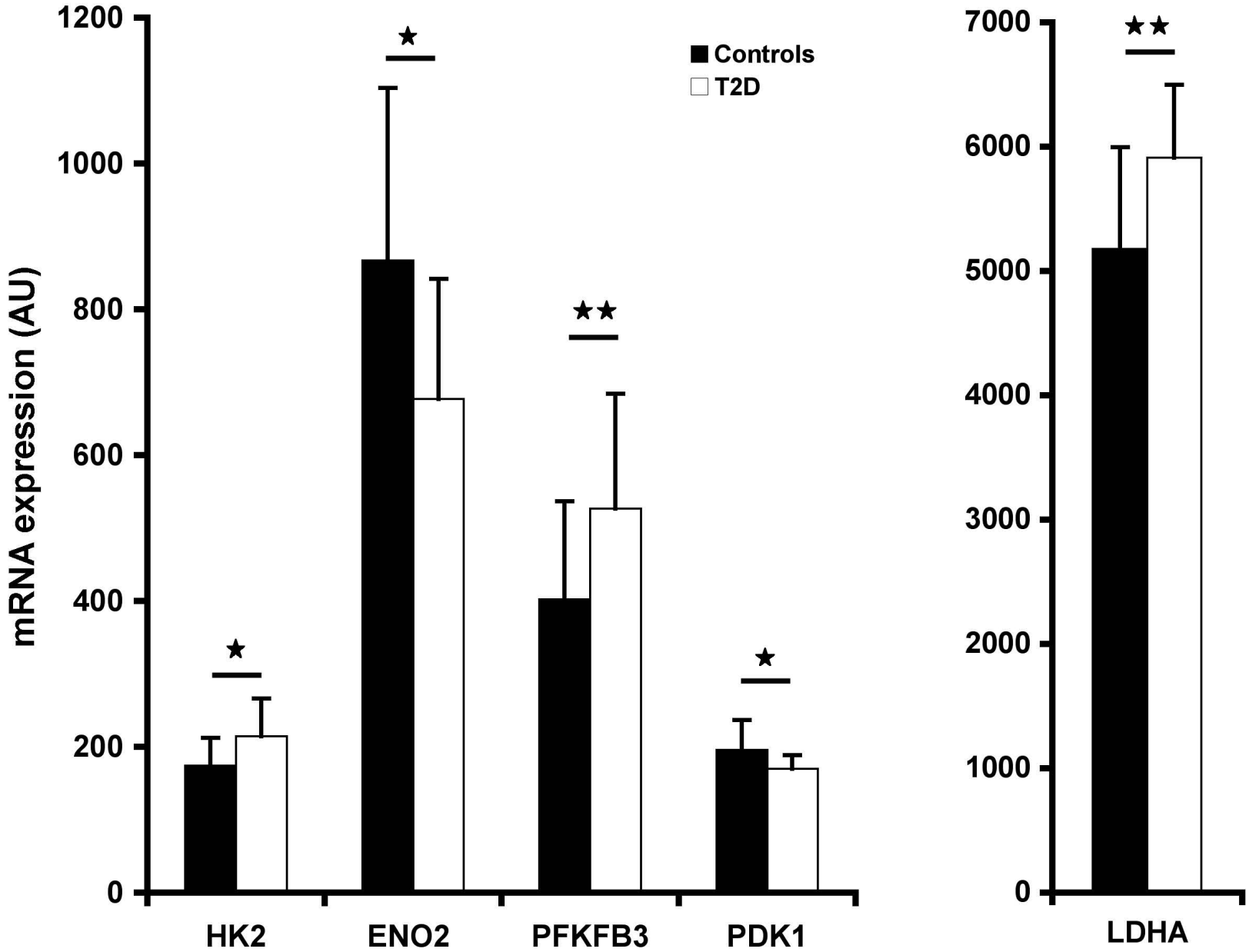
mRNA expression (AU)
1200
1000
800
600
400
200
0
Controls
T2D
★
★
★★
★
HK2
ENO2
PFKFB3
PDK1
7000
6000
5000
4000
3000
2000
1000
0
★★
LDHA

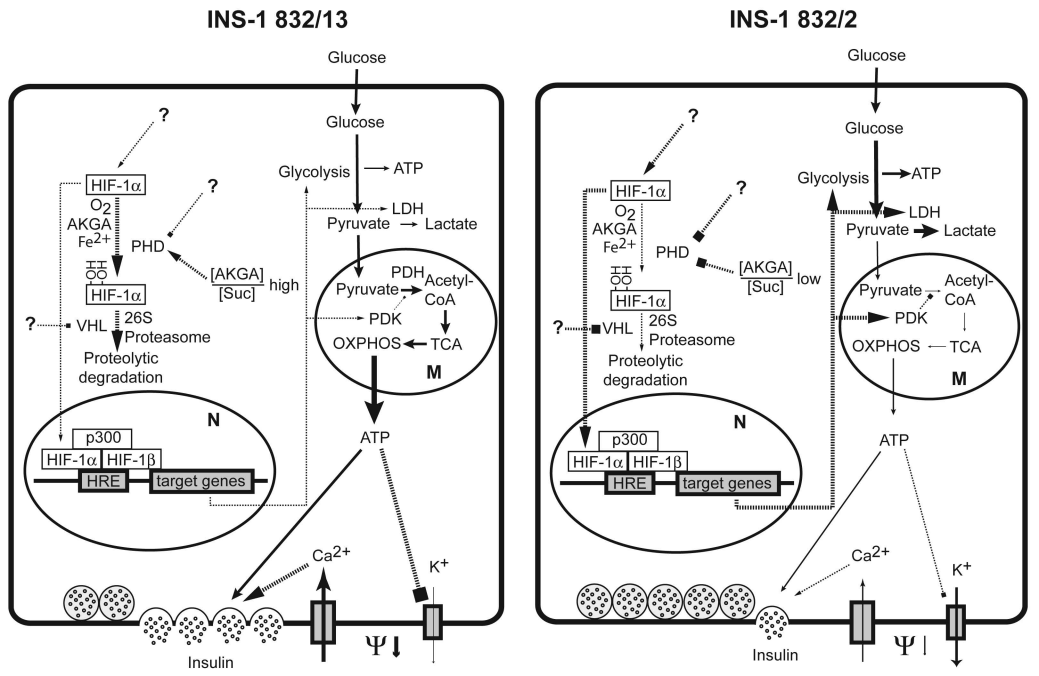
INS-1 832/13
Glucose
Glucose
?
HIF-1α
O2
AKGA
Fe2+
PHD
?
[AKGA]
[Suc]
high
HIF-1α
?
VHL
26S
Proteasome
Proteolytic
degradation
Glycolysis
ATP
LDH
Pyruvate
Lactate
PDH
Pyruvate
Acetyl-
CoA
PDK
OXPHOS
TCA
M
N
p300
HIF-1α
HIF-1β
HRE
target genes
ATP
Ca2+
K+
Insulin
Ψ↓
INS-1 832/2
Glucose
Glucose
?
HIF-1α
O2
AKGA
Fe2+
PHD
?
[AKGA]
[Suc]
low
HIF-1α
?
VHL
26S
Proteasome
Proteolytic
degradation
Glycolysis
ATP
LDH
Pyruvate
Lactate
Pyruvate
Acetyl-
CoA
PDK
OXPHOS
TCA
M
N
p300
HIF-1α
HIF-1β
HRE
target genes
ATP
Ca2+
K+
Insulin
Ψ|

SUPPLEMENTARY ONLINE DATA

Metabolomic analyses reveal profound differences in glycolytic and tricarboxylic acid cycle metabolism in glucose-responsive and -unresponsive clonal β-cell lines

Peter SPÉGEL[*], Siri MALMGREN[*,†], Vladimir V. SHAROYKO[*], Philip NEWSHOLME[‡], Thomas KOECK[*], and Hindrik MULDER[*]

Department of Clinical Sciences in Malmö, [*]Unit of Molecular Metabolism, [†]Unit of Diabetes and Endocrinology, Lund University Diabetes Centre, Malmö, Sweden. [‡]UCD School of Biomolecular and Biomedical Science, UCD Conway Institute and UCD Institute of Sport and Health, UCD Dublin, Belfield, Dublin 4, Ireland.

Running Head: Metabolic regulation in β-cells

Correspondence to: Peter Spégel, PhD, Malmö University Hospital, Clinical Research Center, 91:11:061, 205 02 Malmö, Sweden. Tel.: 0046 40 39-10-21; Fax: 0046 40 39-12-22; E-mail: Peter.Spegel@med.lu.se

INTRODUCTION

Metabolomic analyses generate large amounts of data. Multivariate statistics (chemometrics) has proven to be a powerful tool for evaluation of these large data sets [1]. Unsupervised models, such as principal component analysis (PCA) [2] and supervised models, such as partial least-squares to latent structures (PLS) [3] and orthogonal PLS (OPLS) [4, 5], efficiently highlight similarities and dissimilarities between samples that are due to both single metabolic differences and co-variations. Whereas PCA is focused on describing all systematic variation in the metabolite pattern (X) [6], the regression models PLS and OPLS focus the modelling on differences in X related to some pre-known sample properties of the samples (Y). In PLS, the Y-related variation in X may be difficult to find due to mixing with other Y-independent systematic variations in X. In OPLS, the model is rotated so that the Y-related variation in X is isolated in a predictive component, whereas the Y-independent systematic variations are separated into orthogonal components. This separation into predictive and orthogonal components facilitates interpretation of the data [5]. Furthermore, investigation of the orthogonal components may yield additional information on systematic variations in X.

In the present study, OPLS discriminant analysis (OPLS-DA)-based models were constructed to allow identification and distinction of glucose-dependent and -independent differences between two β-cell lines as well as cell line-dependent and -independent differences in the metabolic response to an elevation of the extracellular glucose concentration. The models comprised regulation of 164 putative metabolites, out of which 44 unique metabolites could be identified.

EXPERIMENTAL

Materials and reagents

N-methyl-N-trimethylsilyltri-fluoroacetamide and methoxyamine hydrochloride were from Aldrich (Steinhein, Germany). Pyridine, heptane, methanol, methyl stearate and the alkane standard mixtures (C_8-C_{20} and C_{21}-C_{40}) were purchased from Fluka (Buchs, Switzerland). The isotope-labeled internal standards $^{13}C_6$-glucose, $^{13}C_3$-^{15}N alanine, $^{13}C_4$-succinic acid, $^{13}C_3$-pyruvic acid, $^{13}C_6$-phenylalanine, $^{13}C_3$-serine, D_7-cholesterol, $^{13}C_{16}$-palmitic acid and $^{13}C_5$-α-ketoisovaleric acid were from Cambridge Isotope Laboratories, Inc. (Andover, MA). The isotope-labeled standards $^{13}C_9$-^{15}N-tyrosine, $^{13}C_{18}$-oleic acid and $^{13}C_4$-octanoic acid were from Isotec (Sigma-Aldrich, St. Louis, MA). Water was purified by Purelab Ultra (Elga, Gothenburg, Sweden). All other reagents and solutions were obtained from Sigma-Aldrich unless otherwise stated.

Cell culture

Clonal β-cell lines (INS-1, INS-1 832/1, INS-1 832/2, and INS-1 832/13) were cultured as previously described [7]. INS-1 832/2 and INS-1 832/13 were seeded in 5 cm tissue culture dishes and INS-1 and INS-1 832/1 were seeded in 12-well tissue culture plates 48 h prior to experiments. Following 48 h pre-incubation, the cells were washed and then kept in SAB supplemented with 2.8 mM glucose for 2 h at 37 °C. The cells were subsequently incubated for 1 h in SAB containing either 2.8 mM glucose or 16.7 mM glucose. After the 1 h incubation period, the cells were washed in ice cold PBS followed by quenching of metabolism by addition of 500 µL -80 ºC methanol to dishes and 300 µL -80 ºC methanol to each of the wells. Cells were scraped off and the volume adjusted with -80ºC methanol; cells in methanol suspension were stored at -80ºC until extracted.

Sample preparation

Metabolites from INS-1 832/2 and INS-1 832/13 cells were extracted by a two phase liquid-liquid extraction. To the cells in methanol suspension, ^{13}C-labeled internal standards, 500 µL chloroform and 500 µL water were added. The metabolites were subsequently extracted in a multitube vortexer (VX-2500 Multi Tube Vortexer, VWR, West Chester, PA) for 10 min, and centrifuged at 5,000Xg for 10 min (Sigma 3K10, St. Louis, MA). 800 µL of the aqueous rich top phase were transferred to new vials containing 0.75 µg methyl stearate and evaporated to dryness in a vacuum centrifuge (miVac Duo concentrator; Genevac, Ipswich, UK) connected to a diaphragm vacuum pump (Vacuubrand, Wertheim, Germany). Metabolites from INS-1 and INS-1 832/1 cells were extracted by a one phase liquid extraction. To the cells in methanol suspension, internal standards and 37.5 µL water were added. The cells were extracted similarly to the other cells; 250 µL of the supernatant were transferred to a GC-vial. Prior to GC/MS analysis, the samples were methoximated by addition of 20 µL 20 mg/mL methoxyamine hydrochloride in dry pyridine. The samples were vortexed for 5 min, and allowed to react at room temperature for 17 h. Finally, 20 µL trimethylsilyl trifluoroacetamide were added and the samples were vortexed for 5 min and allowed to react for an additional 30 min period. For control purposes, a 3 µL aliquot from each sample was pooled and aliquoted to 6 vials. Three blank samples were also prepared.

GC/MS analysis

GC/MS was performed on an Agilent 6890N gas chromatograph (Agilent, Atlanta, GA) coupled to a Leco Pegasus III TOFMS electron impact time of flight (TOF) mass spectrometer (Leco Corp., St. Joseph, MI). Samples (1 µL) were injected in splitless mode using an Agilent 7683B autosampler (Agilent) with an injector temperature of 270 ºC and a vent time of 115s onto a 30 m DB-5 MS column (J&W Scientific, Folsom, CA). After an initial isothermal period at 70 ºC for 5 min, the temperature was ramped 15 ºC/min up to 320 ºC where it was held for 2 min. The transfer line and ion source temperatures were set at 200 ºC and 250 ºC, respectively, and the mass spectrometer was scanning between m/z 50 and 800 with 20 spectra collected per second. Data were acquired using the Leco ChromaTof software (Leco Corp.). All sample preparation and analysis were performed in a randomized order. The vials containing pooled samples which are identical, were run 12 times spread evenly over the entire run sequence to assess any instrumental drift or other technical problems. The three blank samples and n-alkane series (C_8-C_{40}) were analysed in the beginning, in the middle and last in the sequence. Retention indexes were calculated based on the retention times of the homologous n-alkane series.

Data treatment and multivariate analysis

Global analysis: Processing of the raw data, peak identification and normalisation to the ^{13}C stable isotope labelled internal standards were performed according to a previously published protocol [8]. Additional to individual internal standards for normalisation, the scores from the first component of a PCA model constructed in SIMCA P$^+$ 12.0 (Umetrics AB, Umeå, Sweden) from the uncentered and UV-scaled added internal standards [9] was also used for the normalisation method previously described. To adjust for differences in cell number between the samples, normalisation was also conducted using the summarised total ion current (TIC) after removal of the internal standards and artefact peaks identified from

the blank samples. Thus, the total detected metabolome was used for normalisation in an analogous manner to the frequently used normalisation to the total measured proteome. The data matrix containing the normalised peak areas was exported to SIMCA P^+ 12.0 and scaling, centering and transformations were performed as previously described [8]. PCA was used to obtain an overview of the samples and OPLS-DA was used to identify metabolites differing between the two cell lines at the two different glucose concentrations.

Targeted analysis: Data were normalized against protein measured, using the BCA method on the protein pellet generated in the one-phase liquid extraction. The targeted metabolites were further normalized to the first component from a PCA on the uncentered unit variance-scaled internal standards or its isotope-labelled analogoue, when applicable.

RESULTS AND DISCUSSION

Following processing of the data and removal of artefacts, 164 putative metabolites remained out of which 44 unique metabolites could be identified based on data base entries of both mass spectra and retention indices (Table S1). The raw data and the whole data set are posted on the web at http://www.ludc.med.lu.se/research-units/molecular-metabolism/publications/data/aa2f4fbf033bfa07804414e60328fe5e/. A PCA was initially calculated for the purpose of obtaining an overview of the data. The model required 7 components and explained 81.2% of the variation in the metabolome ($R^2(X)=81.2\%$) with a predictability of 71.1% ($Q^2(X)=71.1\%$). No outliers were observed in the data. The score plot clearly showed clustering of the samples in the first two components according to the identity of the cell line and glucose concentration (Figure S1). Thus, the largest variation in the data set was due to the cell line identity and the glucose concentration. However, off-axis clustering of the samples in the PCA score plot severely complicated interpretation of the model. To resolve this problem, an OPLS-DA model was calculated with two responses, i.e., cell line (INS-1 832/2, $Y_1=0$; INS-1 832/13, $Y_1=1$) and extracellular glucose concentration (2.8 mM glucose, $Y_2=0$; 16.7 mM glucose $Y_2=1$). The resulting model was excellent with 2 predictive components, 2 orthogonal components and $R^2(Y)=97.1\%$ and $Q^2(Y)=95.4\%$. In total, 48.2% of the variation in the metabolome data could be related to differences between the cell lines at the two different glucose concentrations ($R^2_p(X_1)=30.2\%$, $R^2_p(X_2)=18\%$). While the model revealed pronounced metabolic differences between the two β-cell lines, their metabolite responses to elevated glucose were quite similar (Figure S2).

To enable identification of differences in the response to elevated glucose and to facilitate the interpretation of the metabolic differences, four individual OPLS-DA models were calculated; 832/2 cells and 832/13 cells at low (A) and high (B) glucose concentrations, 832/2 cells at low and high glucose concentrations (C), and 832/13 cells at low and high glucose concentrations (D). Thus, in each of these models the Y-related variation in X is isolated along one single predictive component. The loadings along the predictive components from these models can then be combined to explain glucose-dependent and -independent differences between the cell lines (combining A and B), and similarities and differences in the response to an elevated glucose level in each of the two β-cell lines (C and D). The model structure is illustrated by the thick arrows in Figure S2.

Glucose-dependent and -independent metabolic differences between the cell lines

First, the metabolic differences between the two β-cell lines were assessed. Model A yielded one predictive and one orthogonal component with $R^2_p(X)=40.7\%$, $R^2(Y)=98.8\%$ and $Q^2(Y)=98.1\%$. Model B yielded the same number of components with $R^2_p(X)=36.3\%$, $R^2(Y)=98.1\%$ and $Q^2(Y)=97.5\%$. The score plots of these models (Figure S3A and S3B) show perfect classification of the samples, indicating pronounced differences in the metabolome of these β-cell lines. Interestingly, shifting positions of the metabolites in the loading plots (Figure S3C and S3D) were observed, clearly revealing that the difference between the cell lines at low and high glucose concentrations was altered. Thus, it is evident that at least parts of the differences between the cell lines were glucose-dependent. To assess which metabolic differences were glucose-dependent and -independent, the correlation loading vectors of the predictive

components from models (A) and (B) were plotted against each other (Figure S4, Table S2). Metabolites found on the diagonal in this plot represent glucose-independent differences between the cell lines, whereas those found in the (-/+) and (+/-) quadrant are those that were glucose-dependent. The loading plots, with jack-knifed confidence intervals (Figure S3C and S3D), show which of the alterations in this plot were significantly different.

Among the metabolites which exhibited different levels in the two β-cell lines regardless of glucose concentration were an unknown reducing disaccharide (yielding a double chromatographic peak due to tautomerization; UDi1 and 2, Figure S5), hydroxyproline, threonine, ribose 5-phosphate, fructose-1-phosphate, lactate, a four carbon sugar alcohol, a five carbon sugar alcohol as well as two unknown compounds, N72 and N91, which most likely were sugars. All these metabolites were higher in the glucose-unresponsive 832/2 cells. In contrast, glycerol 3-phosphate, γ-aminobutyric acid (GABA), glucose, glycine, pyrophosphate, myo-inositol and six unknown metabolites were glucose-independently higher in the 832/13 cells. The unknown metabolites N74 and N97 were most likely sugars, whereas the mass spectra and retention indices of the unknown N102 and N104 suggest that these were disaccharides. The identity of the other two unknowns, N30 and N99, remained unresolved. The TCA cycle intermediate succinate was higher in the 832/13 cells, whereas malate was higher in the 832/2 cells.

Although most metabolic differences between the β-cell lines were independent of glucose, there were some important exceptions. Levels of pyruvate, and the TCA cycle intermediates fumarate, citrate and α-ketoglutarate where higher in the 832/13 cells at high glucose whereas they were lower at low glucose. Furthermore, levels of 3-phosphoglycerate, phosphoenol pyruvate, glucose 6-phosphate and alanine were higher in the 832/2 cells at low glucose. The differential levels of these metabolites at 16.7 mM glucose were largely abolished. Levels of β-alanine and aspartate, the latter involved in the TCA cycle-linked malate-aspartate shuttle, were lower in the 832/2 cells at basal glucose, whereas they were higher at the stimulating glucose concentration. Thus, our models clearly point at significant differences in both glycolysis and the TCA cycle between the glucose-responsive and -unresponsive β-cell lines.

Cell-line dependent and independent differences in metabolic response

To further assess the metabolic difference between the cell lines, models describing the metabolic alterations provoked by a rise of glucose were calculated. Model (C), describing metabolic alterations in the 832/2 cells upon a glucose rise yielded one predictive and two orthogonal components with $R^2_p(X)$==23.4%, $R^2(Y)$=95.8% and $Q^2(Y)$=92.7%. Model (D), describing the same alterations in the 832/13 cells, yielded one predictive and one orthogonal component with $R^2_p(X)$==33.9%, $R^2(Y)$=98.5%, and $Q^2(Y)$=98.1%. Again, the score plots (Figure S6A and S6B) showed a perfect classification of the samples. Most interestingly, a comparison of the loading plots indicated massive shifts of the high loading metabolites (Figure S6C and S6D). To clarify these shifts and to improve the interpretability of these models, the correlating loading vectors of the predictive component were plotted against each other (Figure S7, Table S3). This highlighted cell line-dependent and -independent metabolic alterations provoked by an extracellular glucose rise.

Again, most metabolites were not differentially regulated in the two β-cell lines. Myo-inositol, GABA, and the majority of the identified amino acids decreased, whereas the majority of the sugars and sugar phosphates increased in a cell line-independent manner when glucose was raised. Several unknown metabolites were also found to be cell line-independently regulated. Out of the seven strongest up-regulated metabolites (N65, N73, N84, N86, N98, N100 and N101), the mass spectra and retention indices suggested that six were sugars. The six strongest down-regulated metabolites (N4, N28, N36, N42, N45 and N60) were more heterogeneous and most likely not sugars. However, the late glycolytic intermediates pyruvate and phosphoenol pyruvate were lower in the 832/13 cells at low glucose and higher at high glucose. 3- and 2-phospoglycerate increased with glucose in the 832/13 cells, whereas they were unchanged in the 832/2 cells. Most interestingly, all TCA cycle intermediates identified in the present investigation were found to be cell line-dependently regulated by glucose. Aconitate

was up-regulated in the 832/13 cells, whereas it was unchanged in the 832/2 cells. All other identified TCA cycle intermediates were up-regulated in the 832/13 cells and down-regulated in the 832/2 cells. The unknown disaccharides (UDi1 and 2), which were virtually absent in the 832/13 cells, decreased with increasing glucose in the 832/2 cells. One unknown, N57, which most likely is a sugar, was up-regulated in the 832/13 cells and down-regulated in the 832/2 cells. Two unidentified metabolites, N59 and N75, were up-regulated in the 832/2 cells and down-regulated and unaltered, respectively, in the 832/13 cells. Importantly, raw data plots, reflecting the actual changes in metabolite levels, confirmed the findings of the OPLS-DA model (Figure S8).

Glucose uptake

No significant difference in uptake of the non-metabolizable analogue of D-glucose, 3-O-methyl-D-glucose, could be observed (Figure S9).

References

1 Trygg, J., Holmes, E. and Lundstedt, T. (2007) Chemometrics in metabonomics. Journal of proteome research. 6, 469-479

2 Eriksson, L., Andersson, P. L., Johansson, E. and Tysklind, M. (2006) Megavariate analysis of environmental QSAR data. Part II--investigating very complex problem formulations using hierarchical, non-linear and batch-wise extensions of PCA and PLS. Molecular diversity. 10, 187-205

3 Wold, S. S., M.; Eriksson, L. (2001) Chemom. Intell. Lab. Syst. . 58, 109-130

4 Trygg, J. W., S. (2002) J. Chemom. . 16, 119-128

5 Wiklund, S., Johansson, E., Sjostrom, L., Mellerowicz, E. J., Edlund, U., Shockcor, J. P., Gottfries, J., Moritz, T. and Trygg, J. (2008) Visualization of GC/TOF-MS-based metabolomics data for identification of biochemically interesting compounds using OPLS class models. Analytical chemistry. 80, 115-122

6 Jimenez-Chillaron, J. C., Newgard, C. B. and Gomez-Foix, A. M. (1999) Increased glucose disposal induced by adenovirus-mediated transfer of glucokinase to skeletal muscle in vivo. Faseb J. 13, 2153-2160

7 Hohmeier, H. E., Mulder, H., Chen, G., Henkel-Rieger, R., Prentki, M. and Newgard, C. B. (2000) Isolation of INS-1-derived cell lines with robust ATP-sensitive K+ channel-dependent and -independent glucose-stimulated insulin secretion. Diabetes. 49, 424-430

8 Spégel, P., Danielsson, A., Bacos, K., Nagorny, C., Moritz, T., Mulder, H. and Filipsson, K. (2010) Metabolomic analysis of a human oral glucose tolerance test reveals fatty acids as reliable indicators of regulated metabolism. Metabolomics. 6, 56-66

9 Chorell, E., Moritz, T., Branth, S., Antti, H. and Svensson, M. B. (2009) Predictive metabolomics evaluation of nutrition-modulated metabolic stress responses in human blood serum during the early recovery phase of strenuous physical exercise. Journal of proteome research. 8, 2966-2977

Table S1 Identified metabolites.
Metabolite derivatives identified with the abbreviations used in the 2D-plots, with retention indexes and the standards used for their normalisation.

Table S2 Correlation loading vectors for glucose-dependent/-independent regulation.
Correlation loading vectors of models A and B giving the coordinates of the metabolites in Figure S4.

Table S3 Correlation loading vectors for cell-dependent/-independent regulation.
Correlation loading vectors of models C and D giving the coordinates of the metabolites in Figure S7.

Figure S1 PCA score plot.
PCA score plot showing clustering of the samples according to cell line type and glucose concentration. INS-1 832/2 cells in red and INS-1 832/13 cells in green. H=16.7 mM glucose and L=2.8 mM glucose.

Figure S2 Initial OPLS-DA score plot with information on the final modelling setup
A score plot of the initial two Y-variable OPLS-DA models showing perfect classification of the samples according to cell line type and stimulation condition. H=16.7 mM glucose, L=2.8 mM glucose, INS-1 832/2 cells in red and INS-1 832/13 cells in green. The black arrows in the plot show an overview of the single Y-variable OPLS-DA models. Models **(A)** and **(B)** describe differences between the two cell lines at low and high concentrations of glucose, respectively. Models **(C)** and **(D)** describe the metabolic alterations initiated by a glucose rise in the INS-1 832/2 cells and the INS-1 832/13 cells, respectively. By combining the OPLS loading plots from models **(C)** and **(D)**, differences in the stimulated metabolic response between the two cell lines can be identified and by combining the loading plots from models **(A)** and **(B)** glucose-dependent and -independent metabolic differences between the two cell lines can be identified.

Figure S3 Score and loading plots of the OPLS-DA models describing differences between the cell lines at low and high glucose.
Score and loading plots for the OPLS-DA models describing the differences between the cell lines at low (A) and (C), and high (B) and (D) glucose, respectively. The error bars in the loading plots are generated by jack-knifing. The circle in the score plots indicates the Hotelling´s T2-range. With 80 samples and a 95% confidence interval, four samples can be expected to be found outside this range. Only identified peaks, abbreviated according to table S1, are shown in the loading plots. INS-1 832/2 cells in red and INS-1 832/13 cells in green.

Figure S4 Glucose-dependent and -independent differences between the β-cell lines
A 2D correlation loading plot identifies glucose-dependent and -independent differences between the two cell lines. The double headed arrow indicates metabolites which are different between the lines independent of glucose. Metabolites found on the right portion of the diagonal crossing origin are glucose-independently higher in the INS-1 832/13 cells, whereas the metabolites found in the left portion of the same diagonal are glucose-independently higher in the INS-1 832/2 cells. Metabolites in the top left quadrant are higher in the INS-1 832/2 cells at high glucose and lower at low glucose. The opposite relation is true in the lower right quadrant. Metabolites close to the horizontal axis are at similar levels in the two lines at high glucose and metabolites close to the vertical axis are at similar levels in the two lines at low glucose. Thus, metabolites close to the origin have similar levels in the two cell-lines at both high and low glucose. Only identified metabolites and unknown metabolites discussed in the text are assigned. Abbreviations of metabolites are found in Table S1 and the coordinates of all metabolites in the plot are given in Table S2.

Figure S5 Mass spectra of the presumable disaccharide.
The mass spectra of the two unknown peaks presumably derive from a disacharide. The retention indexes are for peak (A) 2956 and peak (B) 2969.

Figure S6 Score and loading plots for the OPLS-DA models describing metabolic alterations due to a rise in extracellular glucose levels for the two cell lines.
Score- and loading plots for the OPLS models describing metabolic alterations induced by a rise in the extracellular glucose in the glucose-unresponsive INS-1 832/2 cells (A) and (C), and the glucose-responsive INS-1 832/13 cells (B) and (D), respectively. Only identified peaks, abbreviated according to table S1, are shown in the loading plots. Cells cultured at 2.8 mM glucose in green and cells cultured at 16.7 mM glucose in red.

Figure S7 Cell line-dependent and -independent metabolic responses
A 2D correlation loading plot was created from the loading vectors of the OPLS-DA models, which describe metabolic alterations in the INS-1 832/2 and INS-1 832/13 cells brought about by a rise in the extracellular glucose level. The plot is interpreted similarly to the plot shown in Figure 1. Thus, metabolites found on the diagonal are regulated in a similar fashion in the two clonal β-cell lines. Metabolites found in the lower right quadrant are increasing and decreasing upon glucose stimulation in the INS-1 832/13 and the INS-1 832/2 cells, respectively. The coordinates of all metabolites in the plot are given in Table S3

Figure S8 Raw data plots of metabolic alterations
Raw data for metabolites identified by the correlation plots to have differing levels or being differentially regulated in the glucose-unresponsive INS-1 832/2 and the glucose-responsive INS-1 832/13 lines are shown. (**A**) metabolites being more abundant in the INS-1 832/2 cells and explaining the largest glucose-independent differences between the cell lines; (**B**) metabolites being more abundant in the INS-1 832/13 cells and explaining the largest glucose-independent differences between the cell lines; (**C**) TCA-cycle intermediates; (**D**) glycolytic intermediates and metabolites being cell line- or glucose-dependently regulated and not presented in (C); (**E**), unidentified metabolites that are cell line-independently up- or down-regulated by a glucose rise. Abbreviations of metabolites are found in supplemental Table 1. The metabolite levels were normalized to the average of the metabolites in all 80 samples. The p-values are given for INS-1 832/13 low versus high glucose, INS-1 832/2 low versus high glucose and below INS-1 832/2 versus INS-1 832/13 high glucose, INS-1 832/2 versus INS-1 832/13 low glucose. Data are presented as means of this value ±SEM of 20 cell cultures for each condition/cell line (*$p<0.05$, **$p<0.01$, ***$p<0.001$).

Figure S9 Glucose uptake
Uptake of the non-metabolizable analogue of D-glucose, 3-O-methyl-D-glucose assessed in the INS-1 parental clone and the 832/1, 832/1, and 832/13 sub-clones at basal and stimulatory concentrations of 3-O-methyl-D-glucose.

Metabolite	IS	Short	RI	Metabolite	IS	Short	RI
Alanine	Alanine	Ala	1107	Nicotinamide TMS	PCA	Nic	1484
Glycine 2TMS	Alanine	Gly2	1127	Ribose 5P	PCA	Rib5P	2088
Isoleucine 2TMS	Alanine	Ile	1291	Taurine 3TMS	PCA	Tau	1663
Proline 2TMS	Alanine	Pro	1296	Threonine 3TMS	PCA	Thr3	1378
Valine 2TMS	Alanine	Val	1213	Thymine 2TMS	PCA	Thy	1395
Glucose 6P 6TMS peak2	AlphaKeto 1	Gluc6P2	2321	Aspartate 3TMS	Pyruvate	Asp3	1512
3-Phosphoglycerate 4TMS	AlphaKeto 1	Glya3P	1791	Citrate 4TMS	Pyruvate	Cit	1805
Glycerol 2-phosphate 4TMS	AlphaKeto 1	Gly2P	1710	Glutamate 3TMS	Pyruvate	Glu3	1608
Myo inositol 6TMS	AlphaKeto 1	Myo	2080	Lactate	Pyruvate	Lac	1067
Threonate 4TMS	AlphaKeto 1	Thre	1530	Phosphoenolpyruvate 3TMS	Pyruvate	PEP	1587
5-OH sugar alcohol	AlphaKeto 2	5OHs	1703	Putrescine 4TMS	Pyruvate	Putr	1734
Beta-alanine 3TMS	AlphaKeto 2	BAla	1423	Pyrophosphate	Pyruvate	PP	1650
Erythritol 4TMS	AlphaKeto 2	Ery	1503	Pyruvate	Pyruvate	Pyr	1058
Hydroxyproline 2TMS	AlphaKeto 2	OHPro2	1464	Sucrose 6TMS	Pyruvate	Sucr	2616
Glucose Peak1&2	Glucose	Gluc	1897	Unknown disacharide p1	Pyruvate	UDi1	2956
2-Phosphoglycerate 4TMS	Glucose	Glya2P	1764	Unknown disacharide p2	Pyruvate	UDi2	2969
Serine 2TMS	Glucose	Ser2	1257	Uracil 2TMS	Pyruvate	Ura	1336
4-hydroxyproline 3TMS	PCA	OHPro3	1519	Serine 3TMS	Serine	Ser3	1354
Aconitate 3TMS	PCA	Aco	1735	Alpha ketoglutarate MEOX 2TMS	Succinate	AKGA	1566
Adenosine monophosphate	PCA	Aden	3048	Fumarate	Succinate	Fum	1347
Fructose 1P 6TMS	PCA	Fru1P	2278	GABA 3TMS	Succinate	GABA	1526
Glucose 6P 6TMS peak1	PCA	Gluc6P1	2299	Glycine 3TMS	Succinate	Gly3	1305
Glutarate 2TMS	PCA	Glua	1399	Nonanoate	Succinate	Non	1359
Glycerol 3-phosphate 4TMS	PCA	Gly3P	1745	Pyroglutamate 2TMS	Succinate	PGlu	1521
Malate	PCA	Mal	1478	Succinate	Succinate	Succ	1313

ID \ Model	(A) 2.8mM p(corr)[1]	(B) 16.7mM p(corr)[1]
OHPro3	-0,916914	-0,928603
5OHs	-0,824993	-0,705711
Aco	-0,0981377	0,42223
Aden	-0,237975	-0,217586
Ala	-0,490381	0,136095
AKG	-0,696588	0,909255
Asp3	0,876458	-0,849323
BAla	0,68169	-0,605778
Cit	-0,687972	0,782843
Ery	-0,812576	-0,837189
Fru1P	-0,385814	-0,802341
Fum	-0,313315	0,860196
GABA	0,947063	0,894137
Gluc	0,785394	0,889239
Glu6P1	-0,446678	0,0610762
Glu6P2	-0,241469	-0,025615
Glu3	0,129475	-0,372248
Glur	0,175122	0,15809
Glya2P	0,183116	0,461299
Glya3P	-0,890641	0,0949603
Glyc2P	-0,217372	-0,10565
Gly3P	0,915352	0,883103
Gly2	0,845034	0,686078
Gly3	0,763896	0,743638
OHPro2	-0,889345	-0,917434
Ile	0,413027	0,288243
Lac	-0,643104	-0,597302
Mal	-0,621519	-0,367531
MyoI	0,741388	0,524141
N1	0,310018	0,212467
N10	0,752899	0,116564
N100	0,639433	0,488396
N101	0,282104	0,155616
N102	0,959149	0,920315
N103	0,327923	-0,109848
N104	0,947234	0,906722
N105	0,448109	0,219792
N106	0,546142	0,425595
N107	0,667877	0,814484
N108	-0,249876	-0,586027
N109	0,785155	0,734487
N11	0,863468	0,85245
N110	-0,654099	-0,664486
N111	-0,847184	-0,74807
N112	-0,762489	-0,803902
N113	0,753442	0,569499
N114	0,748369	0,792738
N12	0,521262	0,377238
N13	0,188097	0,358044
N14	0,573064	0,347401
N15	0,505805	0,685126

ID \ Model	(A) 2.8mM p(corr)[1]	(B) 16.7mM p(corr)[1]
N16	0,400658	0,315833
N17	0,411399	0,29972
N18	0,468455	0,440135
N19	0,702427	0,741017
N2	0,585679	0,315154
N20	0,619788	0,649258
N21	-0,0459764	0,0783158
N22	0,652667	0,505665
N23	0,362431	0,176044
N24	0,87697	0,79832
N25	0,546729	0,678039
N26	0,852649	0,732558
N27	-0,499111	-0,513407
N28	0,609082	0,619126
N29	-0,344824	0,0678146
N3	0,765662	0,662683
N30	0,943834	0,918214
N31	0,53702	0,69666
N32	0,0840086	-0,722166
N33	0,337146	0,145404
N34	0,403943	0,248856
N35	-0,334835	0,36747
N36	-0,745942	-0,867155
N37	0,419793	-0,480685
N38	-0,588651	-0,782286
N39	0,584795	0,561194
N4	0,0409353	-0,534826
N40	0,759611	0,775946
N41	0,914108	-0,390049
N42	0,901475	-0,345919
N43	-0,567728	-0,220319
N44	0,779131	0,705423
N45	0,812265	0,603715
N46	0,376209	0,697604
N47	0,396235	0,0528043
N48	-0,20415	0,0785049
N49	0,915714	0,881035
N5	0,203863	-0,281202
N50	0,620384	0,553102
N51	-0,078475	-0,537179
N52	-0,807203	-0,442553
N53	0,7366	0,658138
N54	0,745924	0,772491
N55	0,777604	0,655786
N56	-0,745973	-0,13643
N57	-0,877315	-0,156202
N58	-0,606366	0,460119
N59	0,926319	0,857384
N6	0,894604	0,747283
N60	0,83773	0,531551
N61	0,671378	0,572631

ID \ Model	(A) 2.8mM p(corr)[1]	(B) 16.7mM p(corr)[1]
N62	0,0875105	0,320667
N63	0,206561	-0,000493828
N64	0,862737	0,814561
N65	0,182434	0,815453
N66	0,715697	0,572689
N67	0,919729	0,881966
N68	0,71644	0,826515
N69	0,703317	0,526507
N7	0,637055	0,569248
N70	0,586698	0,422333
N71	0,888197	0,909294
N72	-0,862396	-0,946478
N73	0,566506	0,628072
N74	0,930643	0,945451
N75	0,793404	0,501772
N76	0,377086	0,208265
N77	0,613637	0,678469
N78	0,00247163	0,117774
N79	-0,215005	-0,589054
N8	-0,0192987	-0,143481
N80	0,16814	-0,0420653
N81	0,805643	0,604211
N82	-0,851922	-0,456749
N83	0,434558	0,634589
N84	0,83472	0,680033
N85	-0,0166418	-0,237557
N86	0,853292	0,593901
N87	-0,820033	-0,895275
N88	0,0646325	0,739627
N89	-0,0801186	0,0179823
N9	0,837098	0,553132
N90	0,834713	0,850307
N91	-0,89975	-0,944742
N92	0,824516	0,780956
N93	0,23567	0,119989
N94	0,88343	0,847058
N95	0,558217	0,270521
N96	0,506835	0,0813065
N97	0,929298	0,921502
N98	0,563716	0,544638
N99	0,952832	0,932645
Nic	-0,00166197	-0,190262
Non	0,446137	0,268139
PEP	-0,818688	0,0766523
Pro	0,0137675	-0,568871
Put	0,0214021	-0,382393
PGln	0,0103002	0,49462
PP	0,586289	0,768912
Pyr	-0,787967	0,888004
Rib5P	-0,856674	-0,43769
Ser2	-0,0969914	0,164923

ID \ Model	(A) 2.8mM p(corr)[1]	(B) 16.7mM p(corr)[1]
Ser3	-0,0139774	0,182277
Succ	0,613982	0,892013
Sucr	0,674953	0,344472
Tau	0,229216	-0,230475
Thre	-0,662716	-0,398761
Thr3	-0,787614	-0,829057
Thy	-0,66748	-0,853845
UDi1	-0,935339	-0,946349
UDi2	-0,933113	-0,938728
Ura	0,0525348	0,312483
Val	0,240887	0,0345923

ID \ Model	(C) INS-1 832/2 p(corr)[1]	(D) INS-1 832/13 p(corr)[1]
OHPro3	-0,481662	-0,602991
5OHs	0,229794	0,698323
Aco	0,0132	0,399753
Aden	0,117851	0,147779
Ala	-0,549895	-0,0157575
AKG	-0,469246	0,92618
Asp3	-0,55605	-0,933247
BAla	-0,3343	-0,865626
Cit	-0,36961	0,858319
Ery	0,0923518	0,483236
Fru1P	0,911465	0,662269
Fum	-0,501925	0,803657
GABA	-0,664317	-0,858018
Gluc	0,882886	0,900353
Glu6P1	0,740032	0,935065
Glu6P2	0,579901	0,814614
Glu3	-0,273456	-0,693595
Glur	-0,514241	-0,578589
Glya2P	-0,000805723	0,34506
Glya3P	0,133918	0,844295
Glyc2P	-0,432075	-0,281296
Gly3P	-0,330151	-0,369984
Gly2	-0,291101	-0,695826
Gly3	-0,606763	-0,769013
OHPro2	-0,153909	-0,366112
Ile	-0,6189	-0,618879
Lac	-0,11453	-0,0590598
Mal	-0,461279	0,304331
MyoI	-0,578983	-0,776659
N1	-0,0708856	-0,263737
N10	0,0492651	-0,670783
N100	0,948169	0,857172
N101	0,895297	0,821271
N102	-0,396711	-0,605678
N103	-0,335605	-0,608593
N104	-0,305007	-0,548117
N105	0,020967	-0,138476
N106	-0,01192	-0,243702
N107	0,828173	0,817298
N108	0,227026	-0,216934
N109	0,336872	-0,126525
N11	-0,348239	-0,683266
N110	-0,172531	-0,0391102
N111	-0,318205	-0,143311
N112	-0,077306	-0,354723
N113	-0,659808	-0,4918
N114	-0,516227	-0,423244
N12	-0,566381	-0,567342
N13	-0,484235	-0,409641
N14	-0,105207	-0,501379
N15	-0,32267	-0,0963838

ID \ Model	(C) INS-1 832/2 p(corr)[1]	(D) INS-1 832/13 p(corr)[1]
N16	-0,41456	-0,492762
N17	-0,294177	-0,372143
N18	-0,207679	-0,173001
N19	-0,672962	-0,507041
N2	-0,070972	-0,512562
N20	-0,114949	-0,517349
N21	-0,243414	-0,131725
N22	0,174352	-0,205625
N23	0,184695	-0,0745188
N24	0,302894	-0,0680752
N25	-0,698119	-0,441583
N26	-0,156468	-0,405882
N27	-0,438568	-0,147238
N28	-0,723582	-0,738168
N29	-0,764034	-0,352781
N3	-0,422988	-0,375742
N30	-0,0138798	-0,676376
N31	-0,181255	-0,193145
N32	-0,407329	-0,812184
N33	-0,385292	-0,530896
N34	-0,101111	-0,26445
N35	-0,00797608	0,574355
N36	-0,573125	-0,755251
N37	-0,193264	-0,722806
N38	-0,1386	-0,373143
N39	0,236445	0,261467
N4	-0,655941	-0,758539
N40	-0,551757	-0,475293
N41	-0,492404	-0,9648
N42	-0,640672	-0,956899
N43	-0,556367	-0,0842431
N44	0,834817	0,624881
N45	-0,711166	-0,840239
N46	-0,533293	-0,328494
N47	-0,0671095	-0,416596
N48	-0,732327	-0,51294
N49	-0,437092	-0,698887
N5	-0,221354	-0,592214
N50	-0,115084	-0,376108
N51	-0,500988	-0,719908
N52	-0,104118	0,845305
N53	-0,552603	-0,464521
N54	-0,590791	-0,572135
N55	-0,381914	-0,688109
N56	-0,207826	0,543736
N57	-0,619306	0,874914
N58	-0,187801	0,687186
N59	0,384452	-0,766568
N6	-0,369147	-0,798622
N60	-0,682269	-0,916273
N61	-0,218744	-0,419553

ID \ Model	(C) INS-1 832/2 p(corr)[1]	(D) INS-1 832/13 p(corr)[1]
N62	0,0446312	0,281837
N63	-0,642736	-0,671065
N64	0,72119	0,63859
N65	0,867369	0,930474
N66	-0,434034	-0,558133
N67	0,010497	-0,553473
N68	0,820681	0,835781
N69	-0,293422	-0,550744
N7	-0,325301	-0,370463
N70	0,821342	0,750371
N71	-0,321108	-0,216592
N72	-0,33437	-0,129084
N73	0,845092	0,849231
N74	0,0304162	-0,128836
N75	0,55542	-0,161256
N76	-0,494184	-0,563731
N77	-0,641621	-0,659838
N78	0,814894	0,666117
N79	0,00687272	-0,5184
N8	-0,262039	-0,276922
N80	-0,480775	-0,48323
N81	0,190771	-0,487521
N82	-0,157157	0,7932
N83	0,846765	0,786638
N84	0,962205	0,869007
N85	0,593054	0,501626
N86	0,908942	0,861106
N87	-0,00112276	-0,477824
N88	0,751257	0,851326
N89	-0,0594434	-0,0576112
N9	-0,0162407	-0,574508
N90	0,819174	0,544676
N91	-0,61208	-0,57162
N92	0,0384912	-0,488965
N93	-0,187467	-0,342646
N94	0,143924	-0,673276
N95	-0,138367	-0,519545
N96	0,34184	-0,242862
N97	-0,103173	-0,601776
N98	0,913436	0,849985
N99	-0,247574	-0,764405
Nic	-0,279848	-0,510499
Non	-0,641783	-0,725442
PEP	-0,338336	0,708989
Pro	-0,5963	-0,862287
Put	-0,132042	-0,446394
PGln	-0,665955	-0,46176
PP	-0,630812	-0,618672
Pyr	-0,439148	0,914711
Rib5P	0,436967	0,825926
Ser2	-0,0837956	0,218735

ID \ Model	(C) INS-1 832/2 p(corr)[1]	(D) INS-1 832/13 p(corr)[1]
Ser3	-0,462446	-0,159602
Succ	-0,565976	0,462169
Sucr	-0,0963915	-0,424592
Tau	-0,317261	-0,461665
Thre	-0,618901	-0,0777624
Thr3	-0,766011	-0,410846
Thy	-0,071255	-0,359148
UDi1	-0,597559	0,0780098
UDi2	-0,554242	-0,079193
Ura	-0,512003	-0,0713424
Val	-0,656195	-0,578689

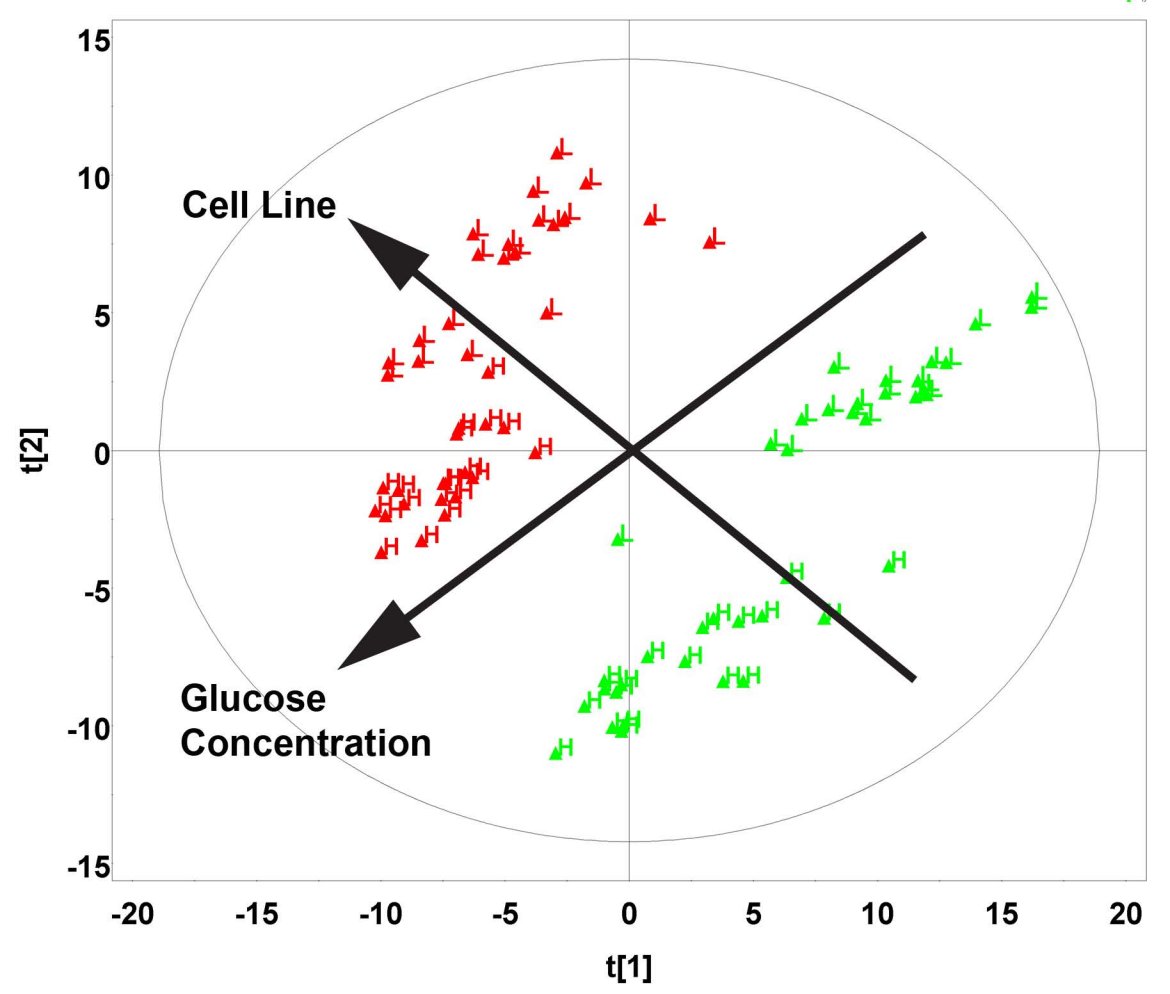
Cell Line
Glucose Concentration
t[1]
t[2]
15
10
5
0
-5
-10
-15
-20
-15
-10
-5
0
5
10
15
20

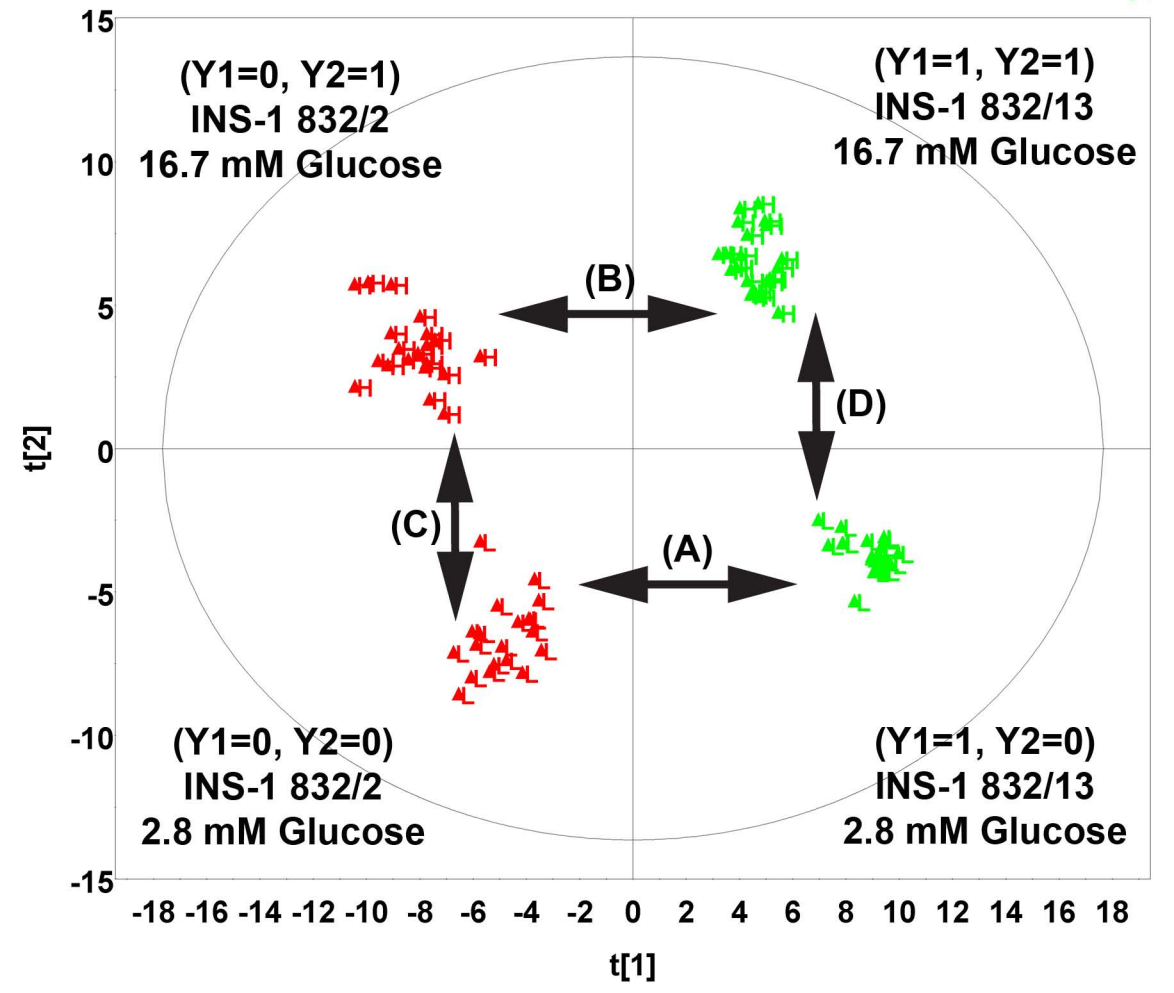
(Y1=0, Y2=1)
INS-1 832/2
16.7 mM Glucose
(Y1=1, Y2=1)
INS-1 832/13
16.7 mM Glucose
(B)
(D)
(C)
(A)
(Y1=0, Y2=0)
INS-1 832/2
2.8 mM Glucose
(Y1=1, Y2=0)
INS-1 832/13
2.8 mM Glucose
t[2]
t[1]
15
10
5
0
-5
-10
-15
-18 -16 -14 -12 -10 -8 -6 -4 -2 0 2 4 6 8 10 12 14 16 18

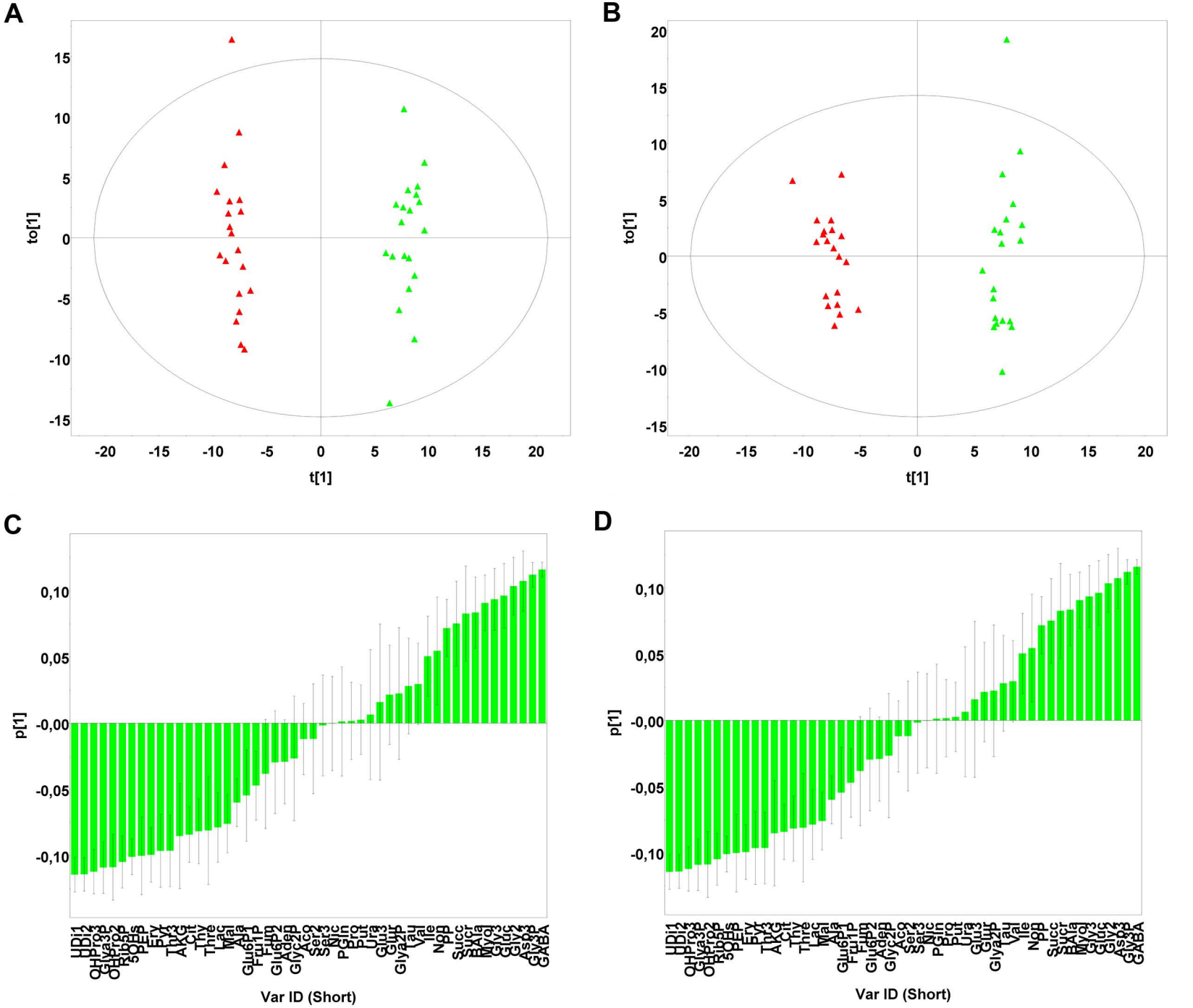
A
B
C
D
to[1]
t[1]
p[1]
Var ID (Short)
UDi1
UDi2
OHPro3
OHPro2
Rib5P
5OPEs
PEP
Ery
Tyr3
AKG
Cit
Thry
Thre
Lac
Mal
Ala
Glu6P1
Fru1P
Fru6P
Glu6P2
Ade2P
Gly2P
Ace2
Ser2
Ser3
Nic
Pgln
Pro
Put
Ura
Glu3
Gly3P
Val
Ile
Npp
Succ
Sucr
BAla
Myo1
Gly3
Gluc
Gly2
Asp3
GABA

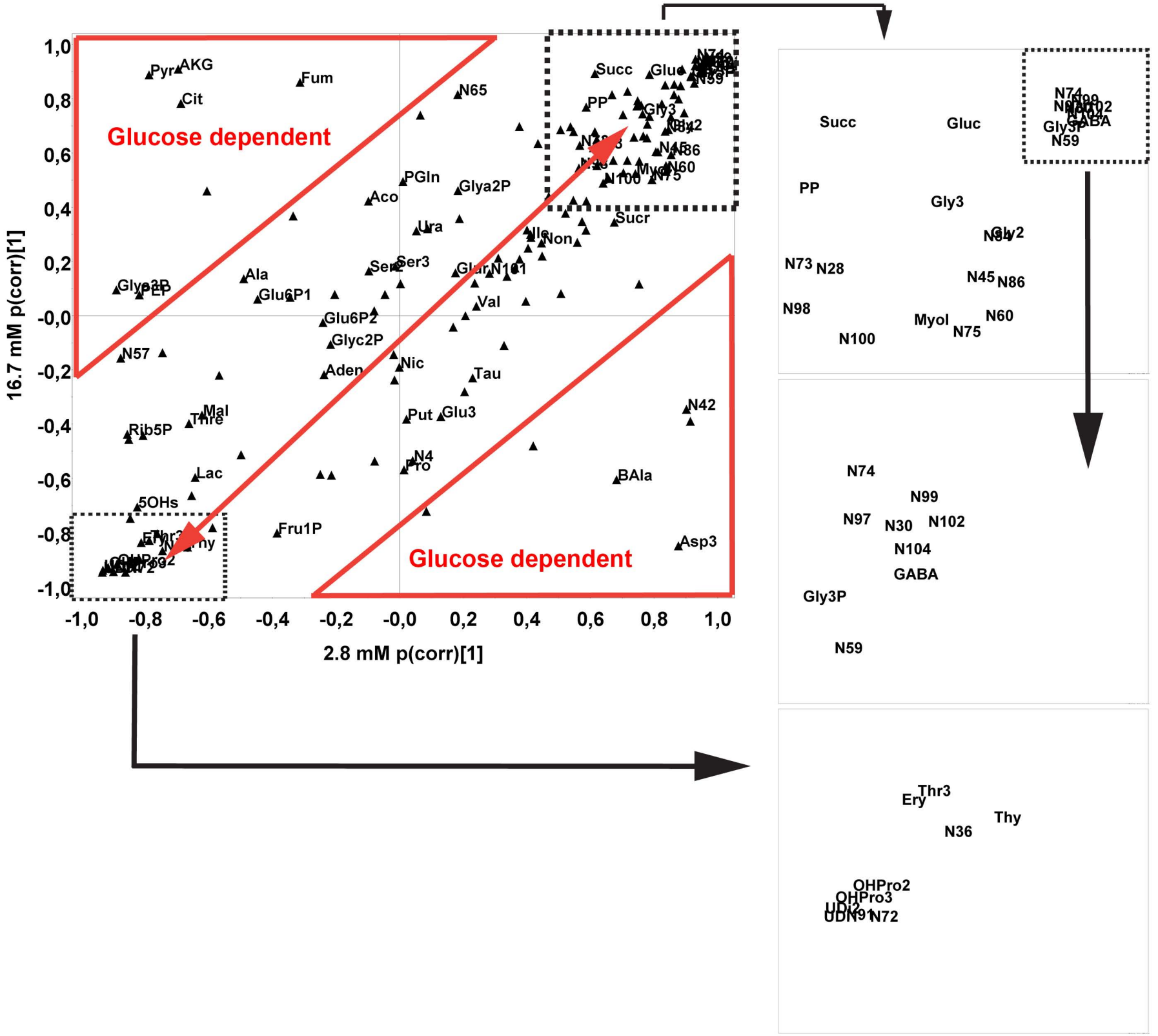
Glucose dependent
Glucose dependent
16.7 mM p(corr)[1]
2.8 mM p(corr)[1]
1,0
0,8
0,6
0,4
0,2
-0,0
-0,2
-0,4
-0,6
-0,8
-1,0
-1,0
-0,8
-0,6
-0,4
-0,2
-0,0
0,2
0,4
0,6
0,8
1,0
Pyr
AKG
Fum
Cit
N65
Succ
Gluc
PP
Gly3
PGln
Glya2P
Aco
Sucr
Ura
Ile
Non
Ser
Ser3
Glut
N101
Ala
Glya3P
PEP
Glu6P1
Val
Glu6P2
Glyc2P
N57
Aden
Nic
Tau
N42
Mal
Thre
Put
Glu3
Rib5P
N4
Pro
Lac
BAla
5OHs
Fru1P
Asp3
Succ
Gluc
PP
Gly3
N73
N28
N45
N86
N98
Myol
N60
N100
N75
N74
N99
N97
N30
N102
N104
GABA
Gly3P
N59
Thr3
Ery
Thy
N36
OHPro2
OHPro3
UDi2
UDN91
N72

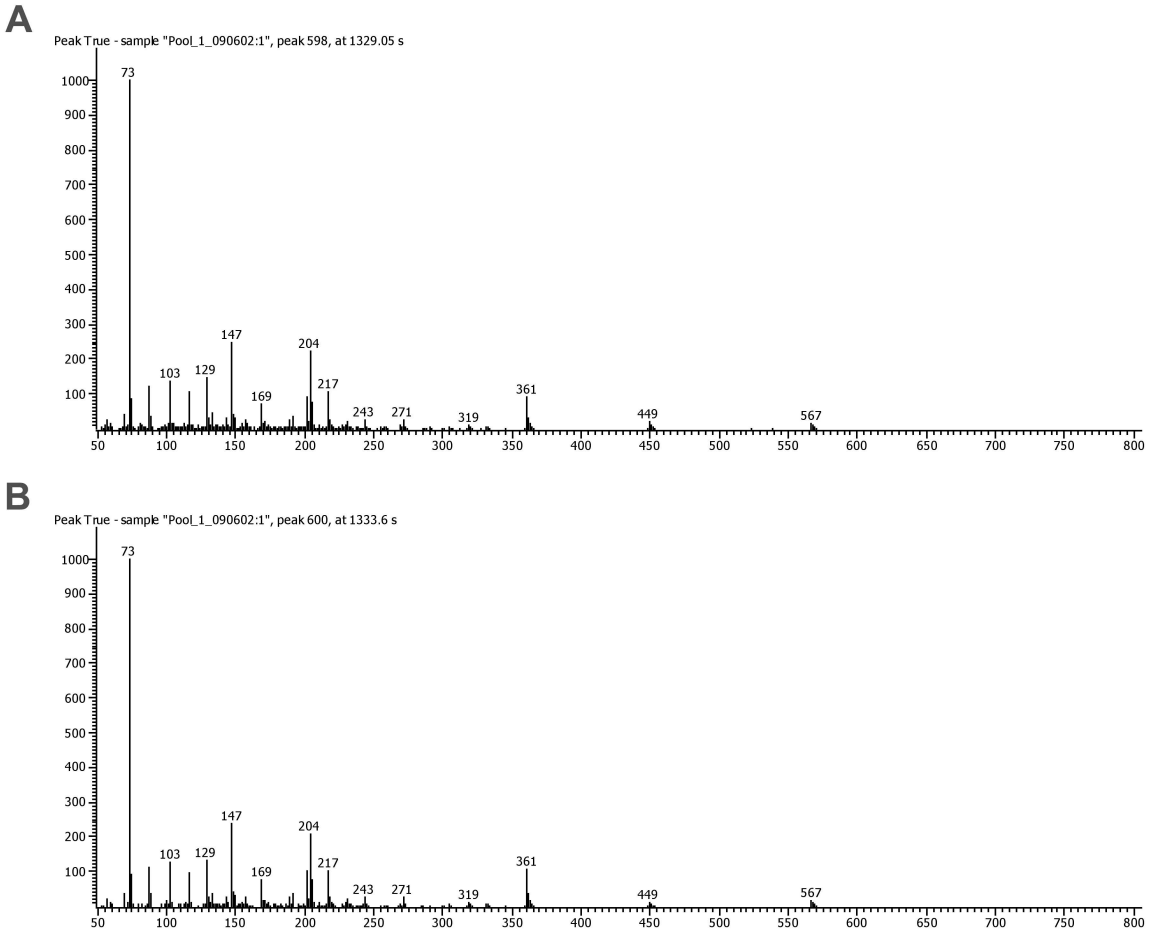
A
Peak True - sample "Pool_1_090602:1", peak 598, at 1329.05 s
B
Peak True - sample "Pool_1_090602:1", peak 600, at 1333.6 s
73
147
204
103
129
217
169
361
243
271
319
449
567

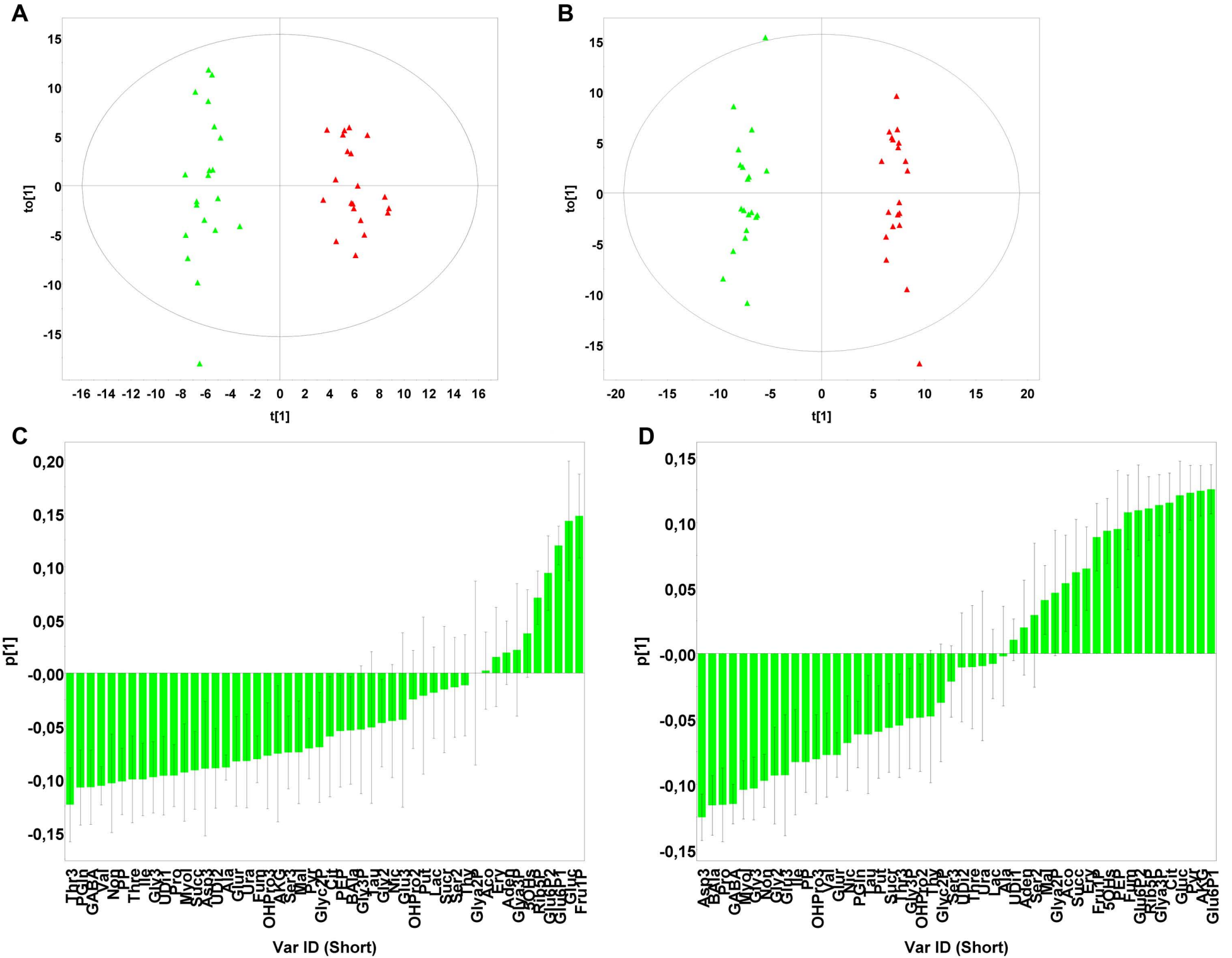
A
B
C
D
to[1]
t[1]
p[1]
Var ID (Short)

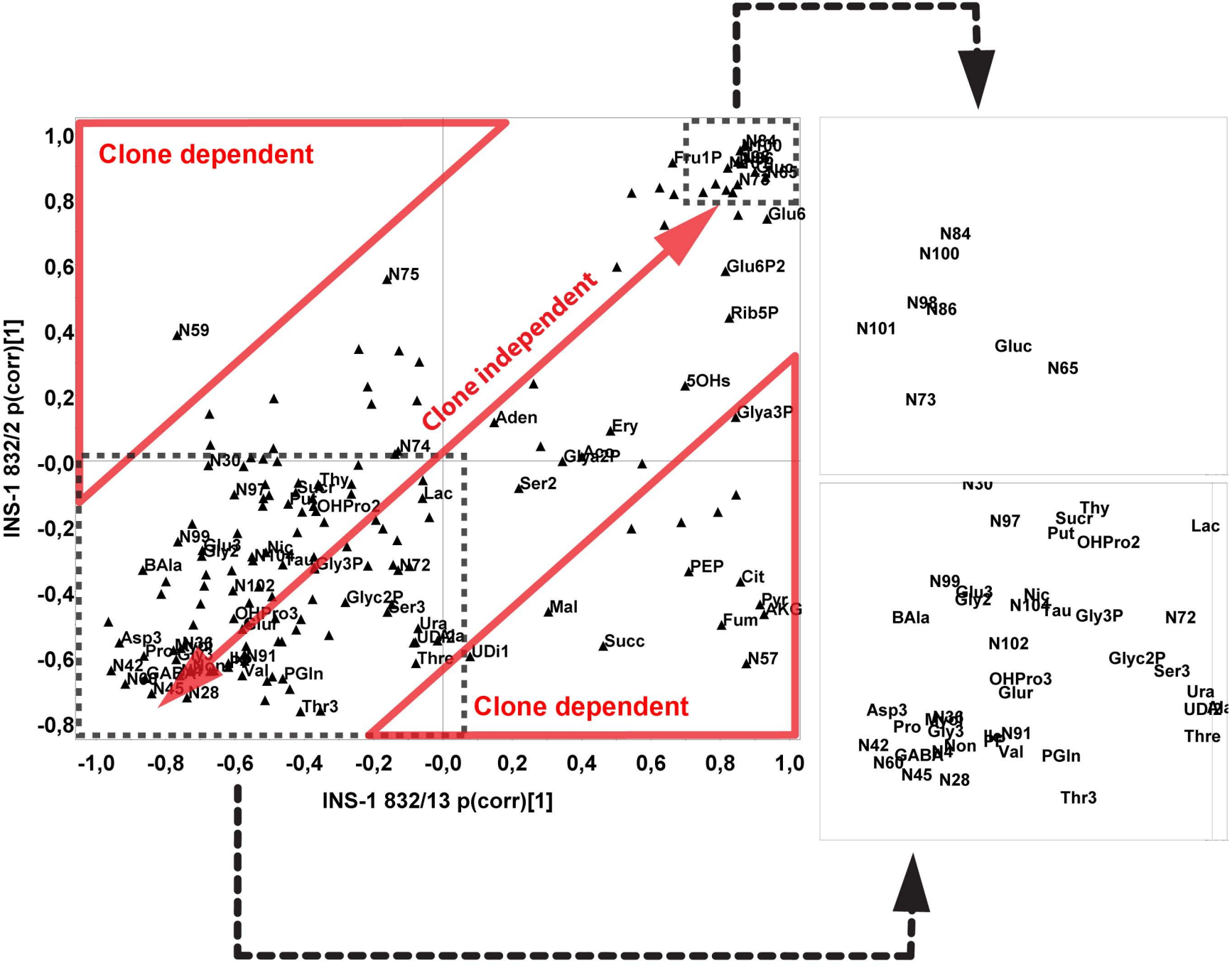
Clone dependent
Clone independent
Clone dependent
INS-1 832/2 p(corr)[1]
INS-1 832/13 p(corr)[1]
1,0
0,8
0,6
0,4
0,2
-0,0
-0,2
-0,4
-0,6
-0,8
-1,0
-0,8
-0,6
-0,4
-0,2
-0,0
0,2
0,4
0,6
0,8
1,0
Fru1P
Glu6
Glu6P2
Rib5P
5OHs
Glya3P
Aden
Ery
Ser2
Lac
PEP
Cit
Pyr
AKG
Fum
Mal
Succ
N57
UDi1
Thre
Ura
Glyc2P
Ser3
Gly3P
N72
BAla
Tau
Nic
Glu3
Gly2
N99
N102
OHPro3
Glur
Asp3
Pro
Val
PGln
Thr3
N42
N45
N28
N59
N75
N74
N30
N97
Thy
Sucr
Put
OHPro2
N84
N100
N98
N86
N101
Gluc
N65
N73

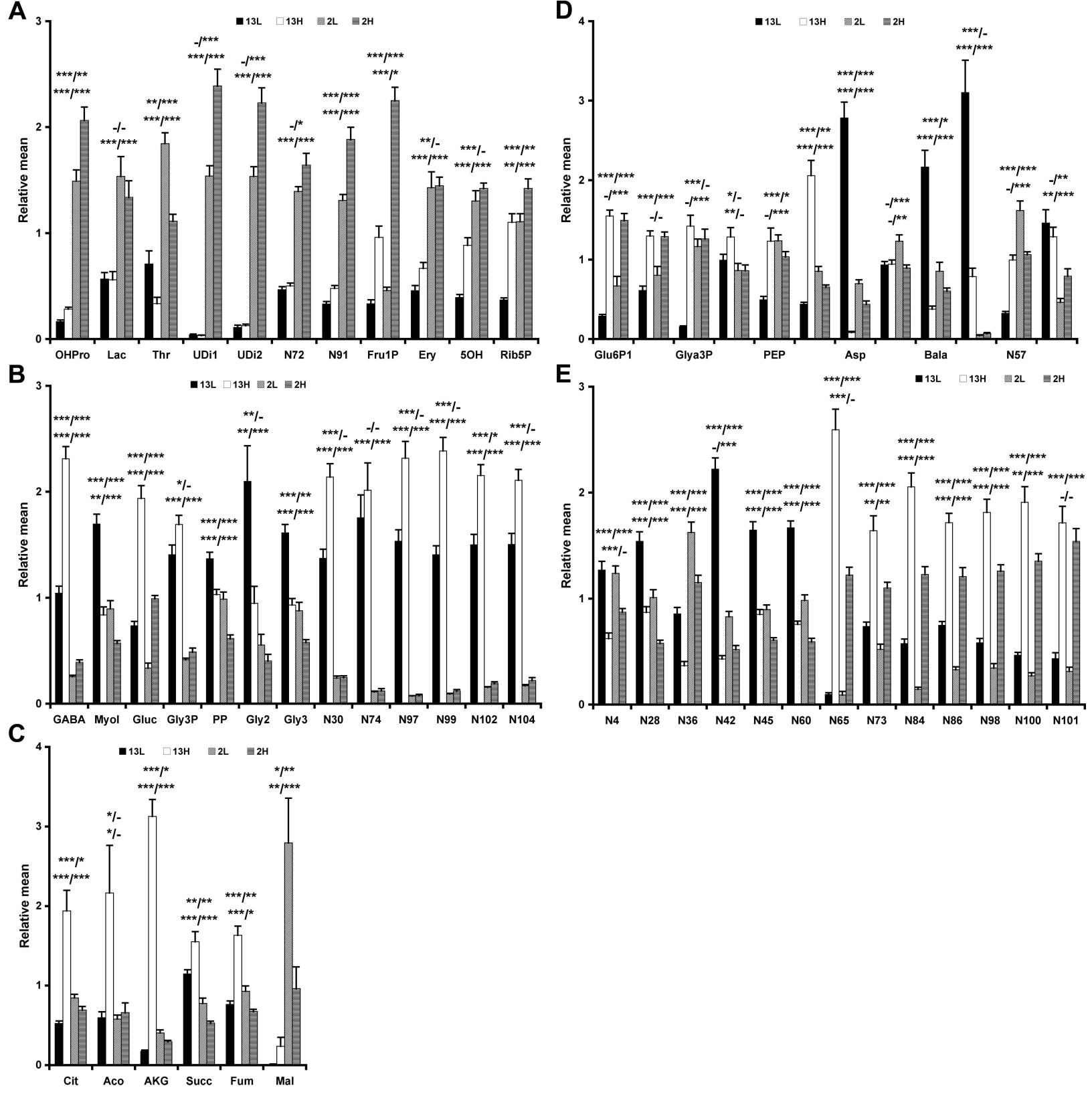
A
B
C
D
E
13L
13H
2L
2H
Relative mean
OHPro
Lac
Thr
UDi1
UDi2
N72
N91
Fru1P
Ery
5OH
Rib5P
GABA
Myol
Gluc
Gly3P
PP
Gly2
Gly3
N30
N74
N97
N99
N102
N104
Cit
Aco
AKG
Succ
Fum
Mal
Glu6P1
Glya3P
PEP
Asp
Bala
N57
N4
N28
N36
N42
N45
N60
N65
N73
N84
N86
N98
N100
N101

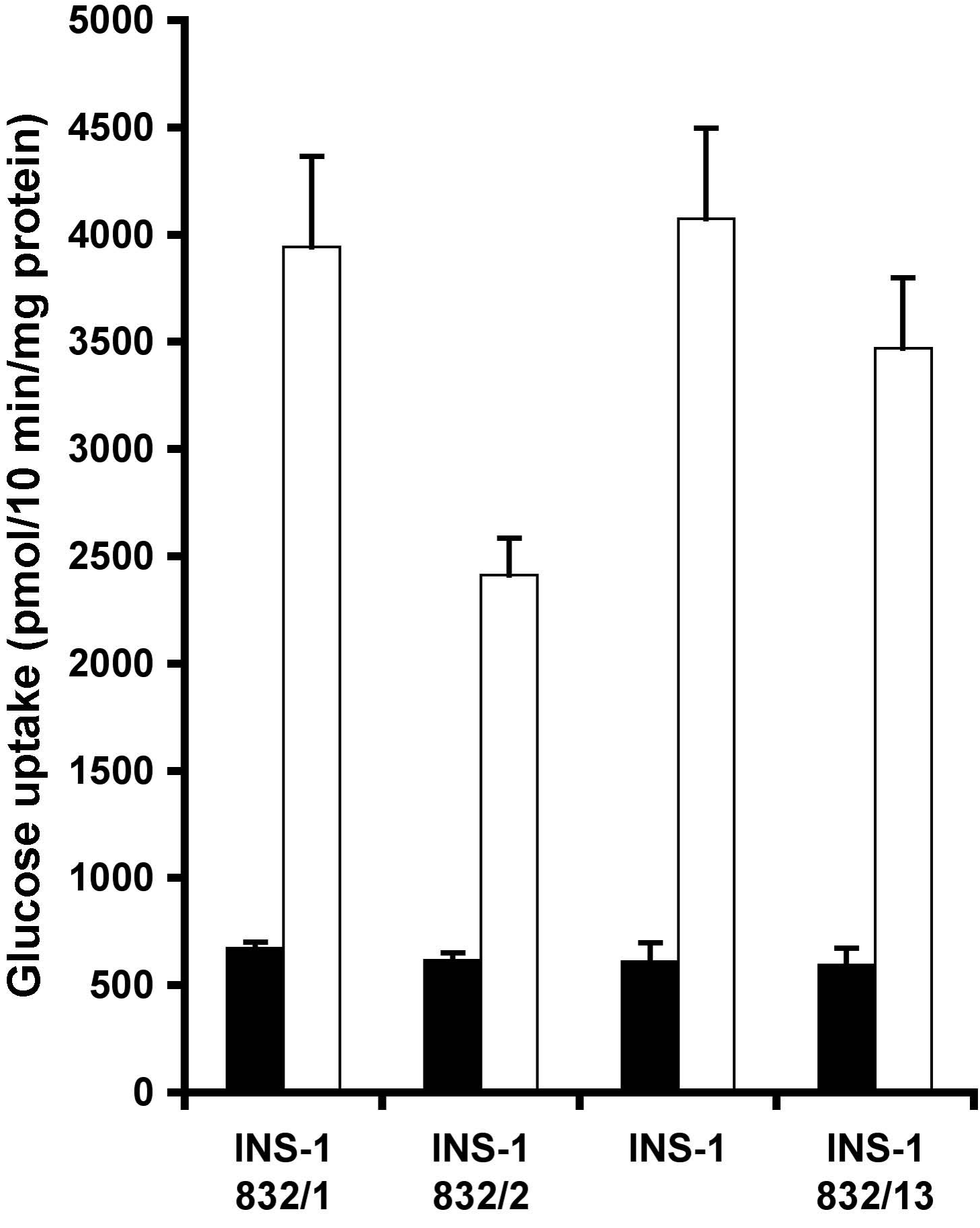
Glucose uptake (pmol/10 min/mg protein)
5000
4500
4000
3500
3000
2500
2000
1500
1000
500
0
INS-1 832/1
INS-1 832/2
INS-1
INS-1 832/13